

ARTICLE OPEN



Synergy between Winter Flounder antimicrobial peptides

Maria Clarke¹, Charlotte K. Hind², Philip M. Ferguson¹, Giorgia Manzo¹, Bhumi Mistry¹, Bingkun Yue¹, Janis Romanopoulos¹, Melanie Clifford², Tam T. Bui³, Alex F. Drake³, Christian D. Lorenz⁴, J. Mark Sutton^{1,2} and A. James Mason¹

Some antimicrobial peptides (AMPs) have potent bactericidal activity and are being considered as potential alternatives to classical antibiotics. In response to an infection, such AMPs are often produced in animals alongside other peptides with low or no perceivable antimicrobial activity, whose role is unclear. Here we show that six AMPs from the Winter Flounder (WF) act in synergy against a range of bacterial pathogens and provide mechanistic insights into how this increases the cooperativity of the dose-dependent bactericidal activity and potency that enable therapy. Only two WF AMPs have potent antimicrobial activity when used alone but we find a series of two-way combinations, involving peptides which otherwise have low or no activity, yield potent antimicrobial activity. Weakly active WF AMPs modulate the membrane interactions of the more potent WF AMPs and enable therapy in a model of *Acinetobacter baumannii* burn wound infection. The observed synergy and emergent behaviour may explain the evolutionary benefits of producing a family of related peptides and are attractive properties to consider when developing AMPs towards clinical applications.

npj Antimicrobials & Resistance (2023)1:8; <https://doi.org/10.1038/s44259-023-00010-7>

INTRODUCTION

In marked contrast to the emergence and spread of resistance to post 1930's antibiotics, antimicrobial peptides (AMPs) have remained an effective component of the innate immune system throughout evolutionary history. Key differences between most antibiotics in clinical use and AMPs are that the latter are rapidly bactericidal, and their dose dependent bactericidal activity is highly cooperative^{1,2}. This desirable pharmacodynamic (PD) property should ensure that a smaller "mutant selection window" exists, minimising the selective pressure associated with an attempted therapeutic response. When resistance to AMPs is evolved experimentally in bacteria, commonly using sub-minimal inhibitory concentration (MIC) conditions, reduced sensitivity can be achieved and there is also a risk of cross-resistance between exogenous AMPs and human defence peptides³. However, such adaptation is relatively modest and may be limited by evolutionary constraints^{4,5}. Therefore, if their enhanced PD properties do indeed mitigate the risk of resistance to AMPs emerging, their rapid production and/or delivery at supra-MIC concentrations would ensure that their utility endures.

Analogous to the use of combination therapies in the clinic to reduce resistance rates⁶, combinations of dissimilar AMPs have been found to have improved PD properties in vitro². However, the AMPs selected were from different organisms and, notwithstanding our own work with temporin L and temporin B from *Rana temporaria*, it is not yet clear the extent to which AMPs from the same organism can combine to improve both antibacterial potency and the cooperativity of the bactericidal activity⁷.

The Winter Flounder (WF), *Pleuronectes americanus*, produces the AMP pleurocidin⁸, whose potent and broad-spectrum antimicrobial activity may be attributed to its dual abilities of both damaging the bacterial plasma membrane^{9,10}, but also crossing it to access intracellular targets^{11–13}. The balance of the contribution of the two effects to the bactericidal action may vary

according to bacterial species and can be impacted by the nutritional environment and hence bacterial metabolism¹⁴. Analogues of pleurocidin that have enhanced membrane disruptive activity may be more robust and are sufficiently potent to be effective therapeutics even when delivered systemically in exacting models of bacterial lung infection¹⁴. Since a pipeline portfolio review, commissioned by the Wellcome Trust¹⁵, "recommends strong support for funding while monitoring for breakthrough insights regarding systemic therapy" for a tier of approaches that include AMPs the potential for pleurocidin and its analogues to be developed further is clear.

Subsequent to the identification of pleurocidin, further WF AMPs were discovered^{16,17}. Antibacterial susceptibility testing of pleurocidin (termed WF2) and five further WF AMPs (sequences given in Table 1) revealed WF1a-1 shared WF2's broad spectrum potency while WF4 had activity towards Gram-negative bacteria only¹⁷. The antibacterial activities of WF1, WF1a and WF3 were modest or absent¹⁷. It is not yet known whether any synergies, in terms of potency or any other parameter, exist between the active or seemingly inactive WF AMPs and hence whether the performance of pleurocidin can be improved or whether other combinations may exceed its potential as a therapeutic. Checkerboard assays are commonly used to identify gains synergistic gains in potency for two-way combinations where growth inhibition with less than half the amount of each component required for inhibition when used alone is commonly taken as defining synergy¹⁸. Such a methodology is cumbersome and inefficient when applied to three-way or higher order synergism and an elegant method has been proposed where the amount of a given antibiotic required to make a small (1%, 5% or 15%) inhibition impact on growth. When these concentrations are mixed in two-way or higher order combinations, there is room for inhibition that surpasses the expected inhibition from additive contributions to be identified for up to at least five-way

¹Institute of Pharmaceutical Science, School of Cancer & Pharmaceutical Science, King's College London, Franklin-Wilkins Building, 150 Stamford Street, London SE1 9NH, UK.

²Technology Development Group, UK Health Security Agency, Research and Evaluation, Porton Down, Salisbury SP4 0JG, UK. ³Centre for Biomolecular Spectroscopy and Randall Division of Cell and Molecular Biophysics, King's College London, New Hunt's House, London SE1 1UL, UK. ⁴Department of Physics, King's College London, London WC2R 2LS, UK.

✉email: chris.lorenz@kcl.ac.uk; Mark.Sutton@ukhsa.gov.uk; james.mason@kcl.ac.uk

Table 1. WF AMP sequences and selected physicochemical characteristics.

Peptide	Sequence	aa	Gly	Charge		$\Delta G_{\text{woct}} - \Delta G_{\text{wif}}$	
				pH 8	pH 2	pH 8	pH 2
WF2/NRC-04 (Pleurocidin)	<u>G</u> <u>W</u> <u>S</u> <u>F</u> <u>F</u> <u>K</u> <u>K</u> <u>A</u> <u>A</u> <u>H</u> <u>V</u> <u>G</u> <u>K</u> <u>H</u> <u>V</u> <u>G</u> <u>K</u> <u>A</u> <u>A</u> <u>L</u> <u>T</u> <u>H</u> <u>Y</u> <u>L</u> -NH ₂	25	4 (16%)	+5	+8	0.391	0.562
WF4/NRC-06	<u>G</u> <u>W</u> <u>S</u> <u>I</u> <u>F</u> <u>K</u> <u>H</u> <u>G</u> <u>R</u> <u>H</u> <u>A</u> <u>A</u> <u>K</u> <u>H</u> <u>I</u> <u>G</u> <u>H</u> <u>A</u> <u>A</u> <u>V</u> <u>N</u> <u>H</u> <u>Y</u> <u>L</u> -NH ₂	25	4 (16%)	+4	+9	0.301	0.587
WF1/NRC-01	<u>G</u> <u>K</u> <u>G</u> <u>R</u> <u>W</u> <u>L</u> <u>E</u> <u>R</u> <u>I</u> <u>G</u> <u>K</u> <u>A</u> <u>G</u> <u>G</u> <u>I</u> <u>I</u> <u>G</u> <u>A</u> <u>L</u> <u>D</u> <u>H</u> <u>L</u> -NH ₂	24	7 (29%)	+3	+6	0.586	0.410
WF1a/NRC-02	<u>W</u> <u>L</u> <u>R</u> <u>R</u> <u>I</u> <u>G</u> <u>K</u> <u>G</u> <u>V</u> <u>K</u> <u>I</u> <u>G</u> <u>G</u> <u>A</u> <u>A</u> <u>L</u> <u>D</u> <u>H</u> <u>L</u> -NH ₂	20	4 (20%)	+4	+6	0.454	0.329
WF1a-1/NRC-03	<u>G</u> <u>R</u> <u>R</u> <u>K</u> <u>R</u> <u>K</u> <u>W</u> <u>L</u> <u>R</u> <u>R</u> <u>I</u> <u>G</u> <u>K</u> <u>G</u> <u>V</u> <u>K</u> <u>I</u> <u>G</u> <u>G</u> <u>A</u> <u>A</u> <u>L</u> <u>D</u> <u>H</u> <u>L</u> -NH ₂	26	5 (19%)	+9	+11	0.659	0.551
WF3/NRC-05	<u>F</u> <u>L</u> <u>G</u> <u>A</u> <u>L</u> <u>I</u> <u>K</u> <u>G</u> <u>A</u> <u>I</u> <u>H</u> <u>G</u> <u>G</u> <u>R</u> <u>F</u> <u>I</u> <u>H</u> <u>G</u> <u>M</u> <u>I</u> <u>Q</u> <u>N</u> <u>H</u> <u>H</u> -NH ₂	24	5 (21%)	+3	+7	0.139	0.377

All peptides were amidated at the C-terminus giving an overall increase in nominal charge of +1. There is 60% identity and 96% similarity between WF2 and WF4 (LALIGN/PLALIGN Waterman–Eggert score: 120; 34.7 bits; $E(1) < 2.2e-08$) and 70 and 85%, respectively, for WF1/WF1a. Average hydrophobicity is given on the whole-residue hydrophobicity octanol-interface scale ($\Delta G_{\text{woct}} - \Delta G_{\text{wif}}$) based on the free energy of transfer from water to palmitoyllecithin phosphatidylcholine and to n-octanol (higher number = more hydrophilic)⁴⁵.

combinations¹⁹. To our knowledge, this method has not yet been applied to AMPs.

Therefore, in the present study we evaluate whether synergy exists in two-way combinations and evaluate the method of Tekin et al. for identifying higher order synergistic combinations of WF AMPs. We test whether synergy affects the in vitro pharmacodynamics that describes their bactericidal activity and determine its impact on outcomes in a *Galleria mellonella* burn wound *Acinetobacter baumannii* infection model. Having established that synergy between WF AMPs is both prevalent and beneficial, both for in vitro PD and in vivo therapy, we use a combination of steady-state and time-resolved biophysical methods to provide mechanistic insight. In particular, we consider how the membrane interaction of selected WF AMPs is affected by the presence of synergistic partners without the formation of hetero-oligomers and how such interactions might underpin both gains in potency but also higher cooperativity in bactericidal action.

RESULTS

Spectrum of antimicrobial activity

We first evaluated the spectrum of antimicrobial activity of the six WF AMPs, using a panel of bacterial isolates that are well characterised and whose susceptibility to other AMPs and membrane active antimicrobials is known (Table 2)^{7,14,20–22}. Because of the marine origin of the WF peptides we also included two representative *Vibrio* isolates, *V. parahaemolyticus* and *V. vulnificus*. Consistent with the previous work of Patrzykat et al.¹⁷, we find that both WF2 (pleurocidin) and WF1a-1 are highly potent antimicrobials, with WF2 displaying the broadest spectrum of activity and WF1a-1 the best Gram-negative activity (MICs 0.25–8 µg/ml), notably for *P. aeruginosa*, (Table 2). To explore this further we prepared D-analogues, to mitigate against proteolytic degradation, and separately tested their activity against an extended panel of *P. aeruginosa* isolates (Supplementary Table 1). The performance of D-WF1a-1 is mostly comparable to that of D-pleurocidin, if not a little better. In contrast with WF2, with which it shares substantial sequence identity (Table 1), the antibacterial activity of WF4 is restricted to Gram-negative bacteria and it is also less active against *Klebsiella pneumoniae* and, as previously¹⁷, ineffective against *P. aeruginosa*. WF4 does however have notable potency against *A. baumannii* and *Vibrio* spp. which is previously undescribed. Again consistent with previous work¹⁷, we find WF1, WF1a and WF3 are largely inactive but both *A. baumannii* strains are susceptible to WF1, highlighting again the general susceptibility of this species to AMPs^{14,20,21}.

Synergy

We used three approaches to explore synergy between WF AMPs. First, we used the method of Tekin et al.¹⁹ to examine the prevalence of two-way and higher order synergy for the WF AMPs against *K. pneumoniae* NCTC 13368 as net Bliss synergy or emergent synergy (Table 3 and Supplementary Tables 2 and 3). Using this methodology, two-way combinations of WF1a/WF1a-1 ($p = 0.002$), WF1a/WF2, WF1a-1/WF3 and WF2/WF3 (all $p < 0.0001$) produced significantly greater growth inhibition than that predicted from an additive combination of each peptide and are thus considered emergent. For higher order conditions, identification of emergent effects, where the synergy is a result of the entire combination rather than an individual pair within the combination, is dependent on identifying growth inhibition that surpasses that achieved with the corresponding lower order synergistic combinations as well as the expected additive effect. However, the ability to identify such emergent effects is impeded in the assay, as presently configured, by the substantial growth inhibition observed for two-way combinations in which each of five of the six WF AMPs are represented (Table 3). This is true even when the individual components produced no detectable inhibition when used alone and likely reflects the highly cooperative and rapidly bactericidal nature of all the WF AMPs. By a less stringent measure of synergy, thirteen of twenty three-way combinations (Table 3), twelve of fifteen four-way combinations and all six-way and five-way combinations produce a significantly greater than additive inhibitory effect (Supplementary Tables 3 and 4).

Then we sought to identify possible synergistic binary combinations for three different bacterial species, selecting antibiotic resistant isolates (EMRSA-15 NCTC 13616, *K. pneumoniae* NCTC 13368 and *A. baumannii* AYE) while validating the approach used above. We used a screening method where two WF AMPs were mixed at a ratio corresponding to their MICs and serially diluted as in a standard broth microdilution assay (Table 4). The two methods are generally in agreement, with the screen also identifying synergy between WF1a/WF1a-1, WF1a/WF2 and WF2/WF3 against *K. pneumoniae* NCTC 13368. The screen additionally suggests one further combination (WF3/WF4) with the discrepancy attributable to the slightly different methodologies and different stoichiometries used in the two approaches. Across the screen of the three isolates, strong synergy (FIC < 0.50) is found for nine of fifteen possible two-way WF AMP combinations, but this is dependent on the bacterial isolate tested. Only two combinations produce synergy against all three isolates—the combinations of WF1a with either WF2 or WF1a-1—with other combinations producing synergy against two or only one of the isolates. The combinations of WF2/WF3 and WF3/WF4 both produce synergy against both Gram-negative isolates. Notably, all six of the WF AMPs participate in at least one synergistic combination and, in

Table 2. Antimicrobial activity.

Isolate	WF1	WF1a	WF1a-1	WF2 (pleurocidin)	WF3	WF4
Gram-negative						
<i>Klebsiella pneumoniae</i> NCTC 13368	32	128	4	4–8	64	16
<i>Klebsiella pneumoniae</i> M6	16	128→128	4	2–8	64	16–32
<i>Acinetobacter baumannii</i> AYE	4–8	16–32	2	2–4	16	2–4
<i>Acinetobacter baumannii</i> ATCC 17978	4–8	16–32	1	2	8–16	2–4
<i>Pseudomonas aeruginosa</i> PAO1	128	>128	2	8–16	>128	64–128
<i>Pseudomonas aeruginosa</i> NCTC 13437	128	>128	4–8	16	>128	128
<i>Pseudomonas aeruginosa</i> RP73	>128	128	8	32	>128	128
<i>Escherichia coli</i> NCTC 12923	4–8	32	1–2	1	8–16	2–4
<i>Vibrio parahaemolyticus</i> NCTC 10903	16	32	0.25	0.5	16	2
<i>Vibrio vulnificus</i> NCTC 13647	32	32	2	1	32	4
Gram-positive						
MS <i>Staphylococcus aureus</i> ATCC 9144	32	128	4–8	2–4	8–32	16–32
EMR <i>Staphylococcus aureus</i> -15 NCTC 13616	128	>128	8–16	16	8–16	>128
EMR <i>Staphylococcus aureus</i> -16 NCTC 13277	128	>128	8–16	4	16–32	128
VS <i>Enterococcus faecalis</i> NCTC 775	128	128→128	128	32–64	64–128	128
VR <i>Enterococcus faecalis</i> NCTC 12201	128→128	>128	128	32	128	128
VR <i>Enterococcus faecium</i> NCTC 12204	128	128	16–32	2–4	32	32–64

Minimal inhibitory concentrations (µg/ml) are given for peptides tested in Mueller–Hinton broth. Italic or bold values indicate, respectively, a significant (factor of >2) reduction or improvement in potency relative to pleurocidin. Modal values are presented from three independently replicates.

MS methicillin sensitive, EMR epidemic methicillin resistant, VS vancomycin sensitive, VR vancomycin resistant.

each of the synergistic two-way combinations found, at least one of the partners has limited or no activity when used alone.

Finally, because in previous work we found that an analogue of pleurocidin with lysine residues replaced with arginine residues and formed of D-amino acids was both robust to serum containing mammalian cell culture media and effective in an in vivo EMRSA-15 NCTC 13616 lung infection model¹⁴, we used Chequerboard assays to see if the D-enantiomer of WF1a (D-WF1a) acts in synergy with D-pleurocidin and/or its analogue D-pleurocidin-KR (Supplementary Table 4). When tested against either EMRSA-15 NCTC 13616 or *P. aeruginosa* RP73 in RPMI (with 5% FBS) strong synergy (FIC < 0.5) is achieved with both combinations. However, in the analogous experiments in MHB synergy is weakened or lost and the data is consistent with subtle changes in mechanism of action or the ability to interact with targets impacting on synergism.

Synergy between WF AMPs enhances cooperativity of bactericidal activity

Above, we consider synergism purely in terms of gains in antibacterial potency but other changes in WF AMP behaviour may emerge because of synergy. In work by others, for two-way and three-way combinations of different AMPs from different organisms kappa, a parameter that describes the cooperativity of the dose dependent bactericidal killing rate, determined in vitro, was found to increase on average for three-way combinations¹. In our own work, again conducted in vitro, we found the cooperativity of the temporin L bactericidal activity against EMRSA-15 NCTC 13616 modestly but significantly increased in the presence of another AMP, temporin B, produced by the same frog⁷. The gain in potency, afforded by synergistic combination of the temporins, is however weak and the cooperativity is lower than that achieved by pleurocidin (WF2) alone in the same conditions⁷.

In the present study we therefore tested whether the in vitro PD profile of WF2 is affected by its much less potent, synergistic partners WF1a or WF3 and compared this with the action of

another WF AMP combination, WF3/WF4, as well as relevant bactericidal antibiotics against three different bacterial isolates in two different conditions (Fig. 1). All WF AMPs and all WF AMP combinations produce substantially faster bactericidal activity than any of the clinically used antibiotics tested, with AMPs killing in minutes and the antibiotics in hours (Supplementary Fig. 1), and this is reflected in the net bacterial growth rates (Fig. 1a, c, e). The maximal killing rate is achieved at or within two times the MIC for ATCC 17978 (Fig. 1a), and approx. ten times the MIC for AYE (Fig. 1c) and EMRSA-15 NCTC 13616 (Fig. 1e). With the exception of gentamicin for *A. baumannii* 17978, which is comparable to all AMPs and AMP combinations, and daptomycin in EMRSA-15 NCTC 13616, which is not inferior to WF2 (but is to D-WF2 and the combination of D-WF2/D-WF1a), this comparison holds also for the cooperativity of the dose dependent activity which is generally much greater for the WF AMPs than what is observed for the clinically used antibiotics (Fig. 1b, d, f).

Since the WF1a and WF3 have relatively weak antibacterial potency, we did not conduct *in vitro* PD experiments for these peptides alone. Therefore, it is moot as to whether the cooperativity of the bactericidal activity for the combinations merely reflects that of the less potent partner or is an emergent property of the combination. Nevertheless, in each of the three separate experiments, the presence of WF1a or its D-enantiomer alongside pleurocidin/WF2 or its D-enantiomer leads to an increase in the cooperativity of the potent and useful bactericidal activity (Fig. 1b, d, f). The presence of WF3 has a similar effect on cooperativity against *A. baumannii* AYE (Fig. 1d) when present with either WF2 or WF4 but this is not observed for ATCC 17978 (Fig. 1b). Further observations include: (1) while the maximal bactericidal killing rate in unaffected, the cooperativity observed for the WF AMPs and combinations is generally lower for the more antibiotic resistant *A. baumannii* AYE (Fig. 1c, d) when compared with the more antibiotic susceptible ATCC 17978 (Fig. 1a, b) and; (2) there is greater cooperativity in the bactericidal action of the D-enantiomer of pleurocidin/WF2 against EMRSA-15 NCTC 13616

Table 3. Bliss independence models of two-way and three-way combinations.

Two-way combinations					Three-way combinations				
Condition	% Inhibition	Additive threshold	Bliss net inhibition	p value	Condition	% Inhibition	Additive threshold	Bliss net	p value
WF1/WF1a	4.26	10.02	-5.76	>0.9999	WF1/WF1a/WF1a1	61.16	26.53	34.62	0.0393
WF1/WF1a1	39.62	21.98	17.64	0.4673	WF1/WF1a/WF2	98.79	16.69	82.10	<0.0001
WF1/WF2	36.06	12.14	23.92	0.1006	WF1/WF1a/WF3	23.58	10.02	13.56	0.9892
WF1/WF3	-1.61	5.47	-7.07	0.9995	WF1/WF1a/WF3	2.63	11.18	-8.54	>0.9999
WF1/WF4	21.45	6.63	14.82	0.7274	WF1/WF1a/WF4	65.6	28.66	36.94	0.0212
WF1a/WF1a1	64.23	21.06	43.17	0.0002	WF1/WF1a1/WF2	73.56	21.98	51.58	0.0003
WF1a/WF2	71.21	11.23	59.98	<0.0001	WF1/WF1a1/WF3	35.09	23.14	11.95	0.9976
WF1a/WF3	4.46	4.55	-0.09	>0.9999	WF1/WF1a1/WF4	87.45	12.14	75.31	<0.0001
WF1a/WF4	-1.57	5.71	-7.28	0.9993	WF1/WF2/WF3	28.07	13.30	14.77	0.9736
WF1a1/WF2	37.72	23.19	14.53	0.7531	WF1/WF2/WF4	11.34	6.63	4.71	>0.9999
WF1a1/WF3	82.53	16.51	66.01	<0.0001	WF1a/WF1a1/WF2	99.24	27.74	71.50	<0.0001
WF1a1/WF4	15.96	17.67	-1.71	>0.9999	WF1a/WF1a1/WF3	92.80	21.06	71.73	<0.0001
WF2/WF3	97.77	6.68	91.10	<0.0001	WF1a/WF1a1/WF4	60.11	22.22	37.88	0.0164
WF2/WF4	12.86	7.83	5.03	>0.9999	WF1a/WF2/WF3	98.70	11.23	87.48	<0.0001
WF3/WF4	-1.16	1.16	-2.32	>0.9999	WF1a/WF2/WF4	78.73	12.39	66.34	<0.0001
					WF1a1/WF2/WF3	99.16	23.19	75.97	<0.0001
					WF1a1/WF2/WF4	36.94	24.35	12.59	0.9955
					WF1a1/WF3/WF4	71.08	17.67	53.41	0.0002
					WF2/WF3/WF4	99.47	7.84	-91.64	<0.0001

The percentage inhibition of *K. pneumoniae* NCTC 13368 in MHB grown in the presence of two-way or three-way combinations of the six WF AMPs according to the method of Tekin et al.¹⁹. Subtraction of the additive threshold— inhibition expected from adding the contributions from non-interacting WF AMPs—from the inhibition achieved provides the Bliss net inhibition. Two-Way ANOVA with Šidák's multiple comparisons test identifies combinations (shown in bold) where the % inhibition significantly surpasses the additive threshold and are synergistic, which for two-way (but not three-way) combinations is emergent. % inhibition and additive thresholds are the average of three independent replicates.

(in RPMI with 5% FBS) when compared with that of the L-enantiomer (Fig. 1e, f).

Synergy between WF AMPs improves therapeutic outcomes

Having established gains in both potency and cooperativity when combining WF AMPs, we sought to establish whether this translated to gains in therapeutic efficacy in an invertebrate burn wound infection (Fig. 2 and Table 5). Larvae of the greater wax moth, *Galleria mellonella*, have been used recently to establish an invertebrate burn wound infection model²³. Using this model we have demonstrated therapy with synergistic combinations of gentamicin and bolalipids and established that gentamicin (5 mg/kg), used worldwide for treatment of infected burn wounds, is protective as a monotherapy²². Here, gentamicin compares favourably with the other three antibiotic interventions (Fig. 2a and Table 5), and the order of therapeutic success (gentamicin > ciprofloxacin > imipenem > meropenem) is the same as the order of the maximal bactericidal killing rate (Fig. 1a).

An intermediate dose of 10 mg/kg WF2 (pleurocidin) offers similar protection to that achieved with 5 mg/kg gentamicin but lower (2.5 mg/kg) or higher (20 mg/kg) doses of pleurocidin do not offer significant protection (Fig. 2b and Table 5). In contrast, similar

levels of protection to that afforded by gentamicin are achieved with low doses (2.5 mg/kg) of WF2 when combined with either WF1a (50 mg/kg) or WF3 (20 mg/kg) with these two AMPs affording no protection when used alone (Fig. 2c and Table 5). Interestingly a combination of 20 mg/kg WF3 and 5 mg/kg WF4 provides complete protection when use of either of these AMPs alone provides none (Fig. 2d and Table 5).

Having established that synergy between WF AMPs leads to gains in potency, an improved pharmacodynamic profile and therapeutic outcomes we asked whether we could obtain any molecular level insights into how this might be effected. It is notable that WF2 and WF4 and, separately, WF1 and WF1a share substantial sequence identities and similarities (Table 1) and yet manifestly differ in their antibacterial properties and ability to participate in synergistic combinations. Since a single AMP is unable to form a pore in lipid membrane by itself, some consider the formation of AMP aggregates essential for their activity²⁴, and synergism for other AMPs has been explained, at least in part, by the formation of hetero-oligomers^{7,25–29}. We therefore conducted a biophysical study of WF AMP conformation and structure as well as their interactions with models of bacterial plasma membranes to characterise and better understand differences in their behaviour and identify aspects that might contribute to synergism.

Table 4. Prevalence of antimicrobial potency synergy in binary combinations of WF AMPs.

Combination	EMRSA-15 NCTC 13616		<i>K. pneumoniae</i> NCTC 13368		<i>A. baumannii</i> AYE	
	FIC (mean ± SEM)	MICs (µg/ml)	FIC (mean ± SEM)	MICs (µg/ml)	FIC (mean ± SEM)	MICs (µg/ml)
WF1/WF1a	1.50	128/128	1.00	16/64	0.50	2/8
WF1/WF1a-1	0.50	32/2	1.00	16/2	0.50	2/0.5
WF1/WF2	0.19 ± 0.06	8/0.25–16/0.5	0.31	8/0.25	0.50	2/0.5
WF1/WF3	0.19 ± 0.06	8/0.5–16/1	0.50	8/16	0.25	1/2
WF1/WF4	2.00	128/128	0.75	16/4	0.75 ± 0.25	2/1 - 4/2
WF1a/WF1a-1	0.38	32/2	0.25	16/0.5	0.25	4/0.25
WF1a/WF2	0.19	16/0.5	0.13	8/0.25	0.25	4/0.25
WF1a/WF3	0.19	16/1	1.00	64/32	0.50	8/4
WF1a/WF4	1.50	128/128	1.00	64/8	0.50	8/1
WF1a-1/WF2	1.50 ± 0.5	4/2–8/4	1.00	2/2	1.00	1/1
WF1a-1/WF3	1.00	4/4	0.50	1/16	0.19 ± 0.06	0.125/1–0.25/2
WF1a-1/WF4	2.00	8/128	1.50 ± 0.5	2/8–4/16	1.00	1/2
WF2/WF3	1.00	2/4	0.25	0.5/8	0.25	0.25/2
WF2/WF4	0.25	0.5/16	1.00	2/8	0.50	0.5/1
WF3/WF4	1.00	4/64	0.25	8/2	0.19 ± 0.06	1/0.25–2/0.5

FICs and the corresponding combination MICs are shown for the simple binary screen. Combinations with FIC < 0.50, i.e. strong synergy, are shown in bold. FICs are the mean of two repeats +/- the SEM where an SEM exists.

WF peptide characteristics

The WF peptides all have the potential to adopt conformations with secondary amphipathicity and are of similar length (Table 1). Of the six peptides, WF3 is noticeably more hydrophobic than the other five peptides, in particular at the N-terminus. WF2, WF3 and WF4 all become more hydrophilic at acidic pH while WF1, WF1a and WF1a-1 conversely become more hydrophobic. All six peptides become more cationic at lower pH. All six peptides are noticeably rich, not only in basic and hydrophobic residues, as is common for cationic amphipathic AMPs, but also in glycine, an amino acid known to confer conformational flexibility.

WF AMPs are characterised by conformational flexibility and can adopt both α -helix and P_{II} conformations

Previously we have shown that pleurocidin does adopt amphipathic α -helix conformations but is less ordered and/or is characterised by substantial conformational flexibility in models that more accurately reflect the ordered plasma membrane^{13,14,30}. Here we present four pieces of evidence that pleurocidin and the other WF peptides can each adopt both α -helix and P_{II} (polyproline-II) conformations.

First, we used far-UV circular dichroism (CD) to study the conformation of all six WF AMPs in aqueous solution as a function of temperature (Supplementary Fig. 2). The spectra obtained at lower temperatures are superficially characteristic of a disordered conformation but on heating there is a substantial change in the spectra of all six AMPs which suggests that at lower temperatures there are contributions to the CD spectra from some ordered or semi-ordered secondary structure. Notably, the intensity of the negative band at 197 nm decreases by almost half while a prominent bump at around 220 nm is also diminished. These features are characteristic of P_{II} conformation even if they are more prominent in model peptides³¹. The spectra obtained at lower temperatures are therefore characteristic of a mixture of disordered and P_{II} conformations, with the latter reduced on heating.

Second, we used far-UV CD to study the conformation of the WF AMPs in three models of bacterial plasma membranes (Fig. 3a–c). In anionic sodium dodecyl sulfate (SDS) micelles, the CD spectra of

all six WF AMPs share characteristics of ordered α -helix conformations with a prominent positive band at 195 nm and negative bands at 208 and 222 nm (Fig. 3a). These however are not as prominent as those observed for temporin L, an AMP with a strong preference for α -helix conformation, and these differences are amplified when the same experiments are performed in lipid bilayers modelling respectively Gram-positive (Fig. 3b) or Gram-negative (Fig. 3c) plasma membranes. The reduction in intensity of these features is consistent both with increased disordering of the α -helix conformation and some adoption of P_{II} conformation with the positive band at 220 nm and negative band at 197 nm expected for P_{II} opposing the spectral features associated with α -helix. Again, the comparison with the CD spectra obtained for temporin L in the same conditions is stark (Fig. 3b, c).

Third, we solved the structures of WF1, WF1a, WF1a-1, WF3 and WF4 in SDS micelles using 2D ¹H-¹H NOESY NMR spectroscopy (Fig. 3f). Notably the half-height linewidths for e.g. the H_N-H_A correlations are much larger than expected and significantly so when compared with those obtained for temporin L (Fig. 3d). Such large linewidths are consistent with slow to intermediate exchange on the NMR timescale. In these scenarios the conformationally dependent chemical shifts from two different conformer populations overlap and/or peptides switch from one conformation to another on the same timescale as the NMR experiment so both conformers are sampled. Consistent with this, *i*-*i*+4 NOEs are detectable but weak and do not extend throughout the peptide sequence (Supplementary Fig. 3) and hence, although a coil motif is evident in the resulting structural models, much less α -helix or 3-₁₀ helix is detected when compared with previously solved structures of temporin L or even pleurocidin (Fig. 3e).

Finally, we conducted triplicate 200 ns atomistic molecular dynamics (MD) simulations of four of each WF AMP binding and inserting into bilayers comprising either 512 POPG or 384 POPE and 128 POPG lipids modelling, respectively, Gram-positive and Gram-negative plasma membranes. We then assessed the intramolecular H-bonding and, over the last 20 ns of each simulation, average Ramachandran angles for each peptide (Supplementary Fig. 4). Consistent with the NMR structural studies, relatively few intramolecular *i*-*i*+4 (or *i*-*i*+3) hydrogen bonds are

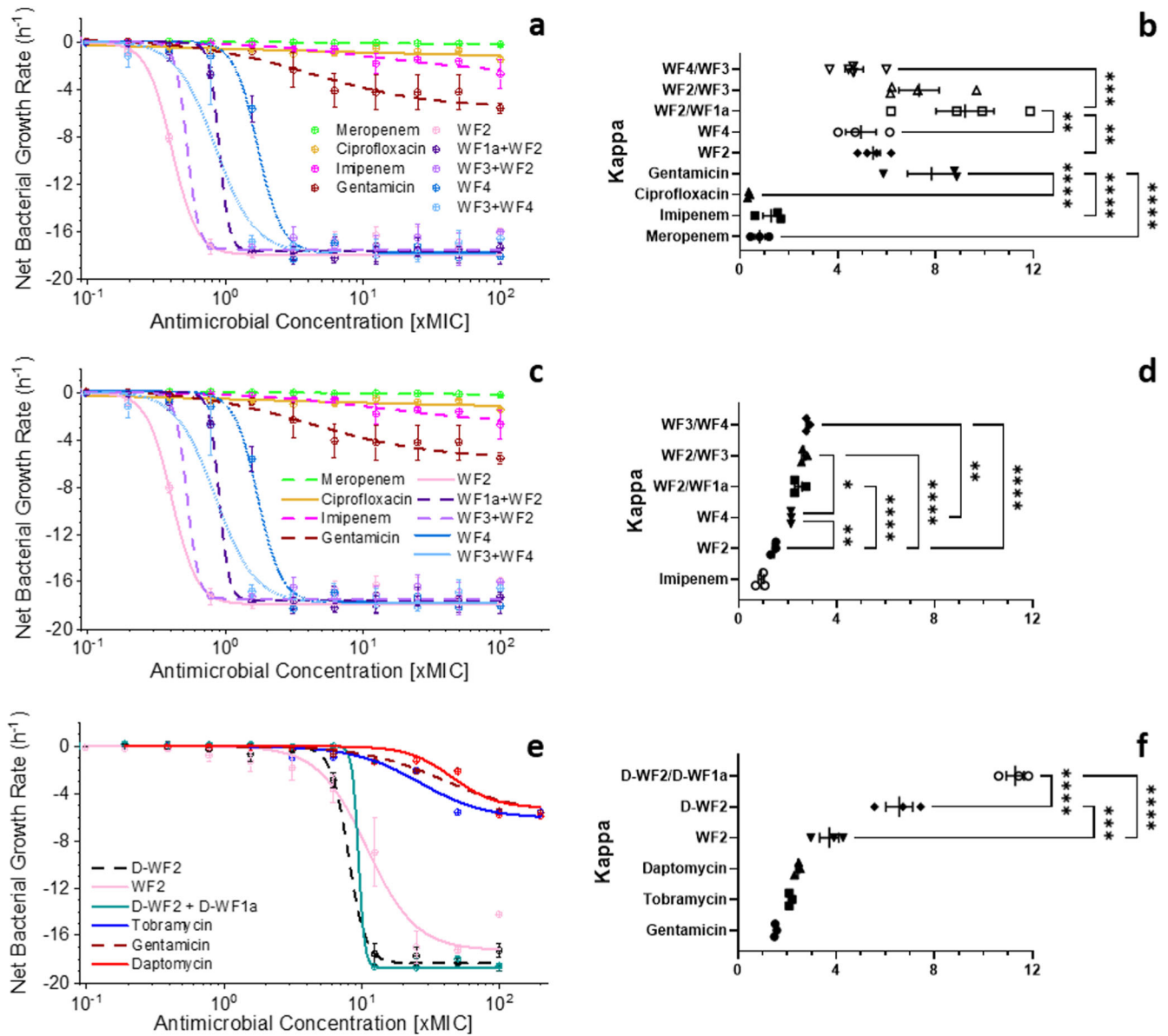


Fig. 1 Winter Flounder AMP bactericidal activity is highly cooperative and can be influenced by synergy. In vitro pharmacodynamics assays performed for selected WF peptides and combinations thereof, and bactericidal, clinically relevant antibiotics to which each strain remains susceptible: *A. baumannii* ATCC 17978 in MHB (**a, b**), *A. baumannii* AYE in MHB (**c, d**) or EMRSA-15 NCTC 13616 in RPMI with 5% FBS (**e, f**) were challenged with increasing concentrations of WF AMPs, WF AMP combinations or clinically relevant antibiotics. Curves shown are fits of averages of three independent repeated experiments (**a, c, e**) and show the change in bactericidal rate as a function of dose, reported as fractions or multiples of the MIC (xMIC). One-way ANOVA with Tukey post hoc test multiple comparisons for Kappa (**b, d, f**), highlight the differences in cooperativity between the WF AMPs, combinations thereof, and antibiotics. Mean and SE of three independent repeated experiments are shown. Only significant pairwise comparisons between AMPs or between clinically used antibiotics are shown (comparisons between AMPs and antibiotics are provided in the main text): * $p < 0.05$; ** $p < 0.01$; *** $p < 0.001$; **** $p < 0.0001$. Selected time-kill curves, used to construct the PD curves in **a**, are provided in the supplementary material (Supplementary Fig. 1).

detected (Supplementary Fig. 4). Again, although of the WF AMPs WF1 and WF2 have higher numbers of $i-i + 4$ hydrogen bonds, in POPE/POPG this is dwarfed by the equivalent measure for the strongly α -helical temporin L (Supplementary Fig. 4B). Less intramolecular hydrogen bonding by WF AMPs relative to temporin L is not offset by increased peptide–lipid hydrogen bonding even if such an effect is observed when replacing lysine residues in WF2 with arginine to create pleurocidin-KR (Supplementary Fig. 4C). Ramachandran plots for WF1a and WF2 (Supplementary Fig. 4D, E) exemplify those observed for the other WFs where individual peptides occupy regions consistent with α -helix ($\varphi -60^\circ$; $\psi -45^\circ$)

and P_{II} ($\varphi -75^\circ$; $\psi +150^\circ$) conformations. As previously established for pleurocidin³⁰, conformational flexibility for the WF AMPs, as determined by the circular variance of φ and ψ is relatively high, particularly as compared here with e.g. temporin L (Supplementary Fig. 5A, B). However, although conformational flexibility of φ for WF1a is reduced when combined with either WF2 or pleurocidin-KR (Supplementary Fig. 5C, D), as exemplified by WF1a and WF2 (Supplementary Fig. 4F), different individual WF peptides are still observed to adopt both conformations in synergistic combinations.

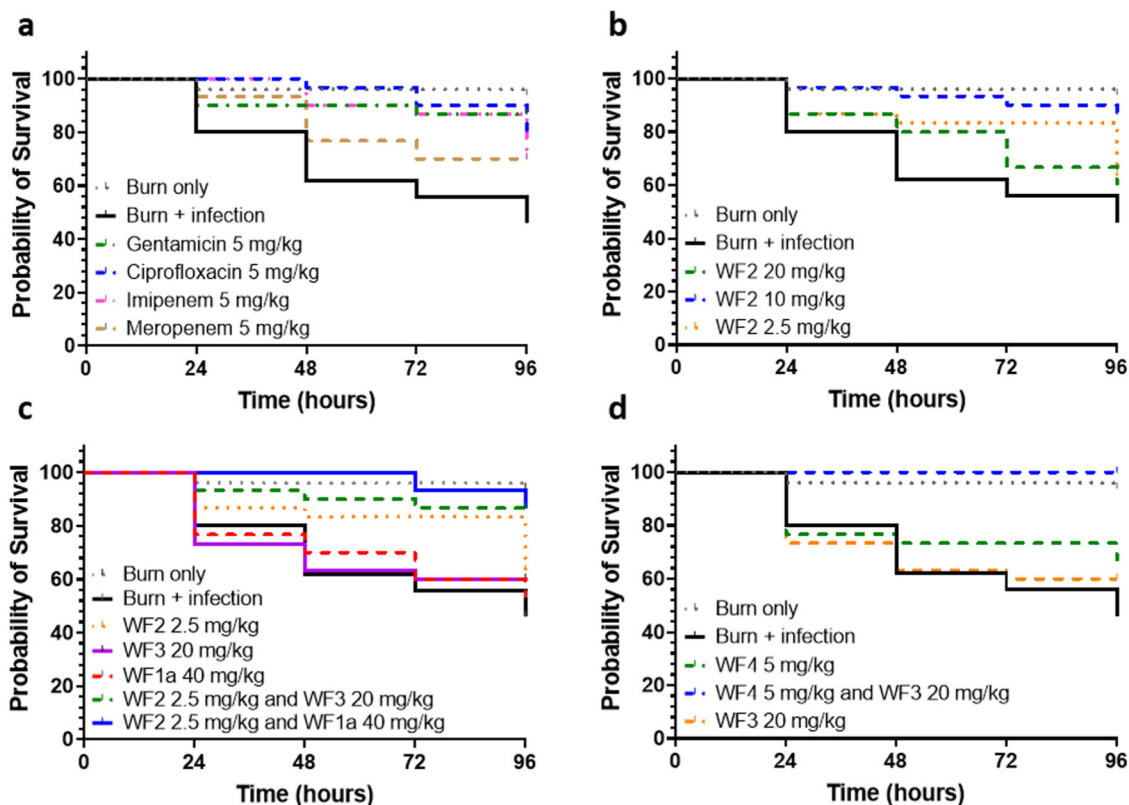


Fig. 2 Winter Flounder AMPs are protective when combined in a *Galleria mellonella* model of *Acinetobacter baumannii* ATCC 17978 burn wound infection. Survival curves are plotted for thirty larvae, each treated with classical antibiotics (a), WF2 (pleurocidin) (b), combinations of WF2 and either WF3 or WF1a (c), or WF3 and/or WF4 (d), in each case compared with fifty larvae subjected to burn only or burn plus infection (*A. baumannii* ATCC 17978) over 96 h. Percentage survival along with significance tests of protection against infection, due to therapy, according to Log-rank (Mantel–Cox) or Gehan–Breslow–Wilcoxon tests are shown in Table 5.

MD simulations reveal differences in bilayer penetration and lipid acyl chain disordering between WF AMPs

analysing the MD simulations further we considered whether there are any differences in penetration of the WF AMPs that might explain their different potencies (Fig. 4). Of note, all six WF AMPs and pleurocidin-KR penetrate more readily into the POPG bilayer when compared with the POPE/POPG bilayer, an effect that is not observed for temporin L (Fig. 4c). In POPG WF2 reaches the level of the lipid phosphates (Fig. 4a) and similar penetration is achieved by pleurocidin-KR but also WF3 and WF4, with penetration by WF1, WF1a and WF1a-1 significantly less (Fig. 4c). In POPE/POPG bilayers, WF2 reaches the interfacial region just above the lipid phosphates (Fig. 4b) and this is similar for all peptides bar WF1.

Indeed, of the three WF AMPs that lack antibacterial potency when used alone, WF1 penetrates significantly less into either bilayer than any of the other peptides but WF3 penetrates readily and WF1a penetrates as much as its much more potent analogue, WF1a-1, even if less than WF2 in POPG (Fig. 4c).

To assess the impact on the bilayers of the peptide penetration we calculated lipid acyl chain order parameters for lipids within 4 Å of each inserting peptide. For POPG bilayers, all WF AMPs induce increased disordering (Supplementary Fig. 6A). In the mixed POPE/POPG bilayers, disordering of the anionic PG component due to WF AMPs is similar in the hydrophobic core (between carbons 6 and 14) but WF2 (pleurocidin) disorders the acyl chains more than the other WF AMPs in the region closer to the headgroup (Supplementary Fig. 6B). The disordering effect is generally greater for the PE component and is similar for all WF AMPs except for WF3 which induces greater disorder in the hydrophobic core (Supplementary Fig. 6C).

In previous simulations of eight temporin L peptides binding to the same bilayers as used in the present study we observed long lasting assemblies of three, four or five peptides⁷. Here, with half as many peptides in each simulation the formation of assemblies is less likely though at least one dimer is formed for at least 50 ns by all WF AMPs bar WF3 (Supplementary Figs. 7 and 8). Assemblies are less likely for pleurocidin-KR relative to WF2 but more likely for WF4 and WF1a, with a long-lasting trimer forming in one WF1a simulation (Supplementary Fig. 7). Even though WF3 eschews aggregation when unmixed, in combination a trimer forms and endures in one simulation indicating that hetero-oligomers are possible (Supplementary Fig. 8A). WF AMPs can therefore assemble into dimers, but higher order assemblies are rare at the current peptide surface density.

Penetration, acyl chain disordering and peptide-lipid hydrogen bonding are altered when WF AMPs are combined

to determine whether any of the properties described above are altered when WF AMPs are present in synergistic combinations, analogous MD simulations were performed where two of each WF AMPs were mixed per the following combinations: WF1a/WF2 in POPE/POPG bilayers (Fig. 5); WF1a/WF2 and WF1a/pleurocidin-KR in POPG bilayers and WF1a/pleurocidin-KR, WF2/WF3 and WF3/WF4 in POPE/POPG bilayers (Supplementary Figs. 9–13).

This maintains the overall number of WF AMPs challenging each bilayer—four—but reduces the number of each type of WF AMP in each simulation. Whereas penetration of WF AMPs, when unmixed, is very consistent between replicate simulations (Fig. 4c), when combined the penetration becomes more variable between replicates and between peptides in each simulation. While some WF2 AMPs penetrate the POPE/POPG bilayer to the same extent

Table 5. Survival of ATCC 17978 burn wound-infected *Galleria mellonella*.

Condition	Survival % @ 96 h	p value	
		Log-rank (Mantel–Cox) test	Gehan–Breslow–Wilcoxon test
Burn only	95.0	<0.0001	<0.0001
Gentamicin 5 mg/kg	86.7	0.0006	0.0013
Ciprofloxacin 5 mg/kg	80.0	0.0017	0.0009
Imipenem 5 mg/kg	70.0	0.0169	0.0084
Meropenem 5 mg/kg	70.0	0.0419	0.0488
WF2 (pleurocidin) 20 mg/kg	60.0	0.2082	0.2633
WF2 (pleurocidin) 10 mg/kg	86.7	0.0004	0.0004
WF2 (pleurocidin) 2.5 mg/kg	63.3	0.0897	0.0813
WF1a 50 mg/kg	53.3	0.5844	0.6668
WF2 2.5 mg/kg/WF1a 50 mg/kg	86.7	0.0002	0.0001
WF3 20 mg/kg	60.0	0.3653	0.6120
WF2 2.5 mg/kg/WF3 20 mg/kg	86.7	0.0005	0.0009
WF4 5 mg/kg	66.7	0.1091	0.1984
WF3 20 mg/kg/WF4 5 mg/kg	100.0	<0.0001	<0.0001

Significance tests are versus burn and infection where survival at 96 h is 46.0%. Conditions where significant ($p < 0.05$) protection is afforded by the treatment are highlighted in bold. Burn only and burn + infection $n = 50$, all treatment groups $n = 30$.

as when unmixed, some peptides penetrate much further into the bilayer in the presence of WF1a (Fig. 5a), with part of the peptide penetrating for the first time beyond the plane of the phosphates (Fig. 5b). The same effect is observed for the combination of WF1a and pleurocidin-KR in POPG bilayers (Supplementary Fig. 9A) with similar behaviour observed for WF2 with WF1a in POPG (Supplementary Fig. 9A) and pleurocidin-KR and WF1a in POPE/POPG (Supplementary Fig. 10B) even if there is no significant increase in average penetration. Penetration of POPE/POPG by WF2 is not affected by the presence of WF3 in the same way (Supplementary Fig. 12A) but WF4 does penetrate further when combined with WF3 (Supplementary Fig. 13A), reaching below the lipid phosphate plane (Supplementary Fig. 13C).

For the combinations of WF1a/WF2 and WF2/WF3, disordering of POPG but not POPE lipids is attenuated (Fig. 5b, d and Supplementary Fig. 12B, D), with a similar but less pronounced effect for WF1a/pleurocidin-KR (Supplementary Fig. 11B, D). Disorder induced by the WF3/WF4 combination is broadly similar to that achieved by the unmixed peptides (Supplementary Fig. 13B, D), as is that achieved with the WF1a/WF2 and WF1a/pleurocidin-KR combinations in POPG (Supplementary Figs. 9B and 11A).

To gain insight into the mechanism underpinning these changes in behaviour we considered how the WF AMPs are interacting with the bilayers by quantifying peptide-lipid hydrogen bonding by residue over time (Figs. 5e–h and Supplementary Fig. 9, 10, 12, and 13). While the total number of hydrogen bonds between the peptide and lipids does not change between the unmixed and combination conditions, the pattern observed for WF2 while inserting into POPE/POPG bilayers in the combination is substantially altered while that for WF1a is unaffected (Fig. 5e–h). Notably, strong interactions between lipids and His11 and Lys14 in particular and also Lys8 and His15, that are characteristic of WF2 insertion when unmixed (Fig. 5g), are absent or diminished when in combination with WF1a (Fig. 5h). In contrast, hydrogen bonding at the C-terminus (Thr22, His23, Tyr24) is enhanced (Fig. 5g, h).

The same effect is observed for WF2 inserting into POPG bilayers in the presence/absence of WF1a (Supplementary Fig. 9C–F) and for the analogue pleurocidin-KR inserting into either bilayer, again in the presence of WF1a (Supplementary Fig. 10C–J).

For pleurocidin-KR the effect is more dramatic due to the stronger hydrogen bonding potential of its four arginines over the original lysines in WF2/pleurocidin. The presence of WF1a therefore alters the peptide-lipid hydrogen bonding pattern of any peptide that is based on the pleurocidin template. Interestingly the hydrogen bonding pattern of WF2 is also affected by the presence of WF3 (Supplementary Fig. 12E–H) and the same effect is observed for WF4 with which WF2 shares substantial sequence identity and similarity (Supplementary Fig. 13E–H).

In both cases the hydrogen bonding pattern observed for WF3 is unaffected by the presence of either WF2 or WF4, but for both of these peptides the presence of WF3 leads to a substantial enhancement of hydrogen bonding mediated by Gly13/Lys14 (WF2) or Ala13/Lys14 (WF4) at the expense of other interactions which dominate when the peptides are unmixed. As such the MD simulations reveal that less active WF AMPs can modulate the mechanism by which more active WF AMPs interact with lipid bilayers but as yet there is no evidence for the reverse.

WF AMP synergism is reflected in enhanced membrane activity in ion conductance measurements

Finally we investigated whether the atomic level understanding of the WF AMP membrane interaction afforded by the MD simulations could be related to effects that might be more readily associated with bactericidal activity and the extent to which membrane activity can explain antimicrobial potency and synergy. Indeed, notwithstanding the ability of pleurocidin to penetrate within bacteria to reach intracellular targets^{11,12}, it has well-established membrane disruptive properties^{9,32}, and both membrane damage and penetration behaviours may be revealed by appropriate ion conductance measurements.

In the patch-clamp experiments our approach has been to titrate peptide to find the lowest threshold concentration capable of triggering ion conductance and then to characterise this membrane activity both qualitatively and quantitatively^{7,14,20,21}. Interestingly this threshold concentration, obtained for WF AMPs challenging diphytanoyl lipids, is correlated to the average disordering of the corresponding palmitoyl-oleoyl lipids in the MD simulations (Fig. 6a). A similar but weaker relationship may exist between penetration (COM) and the threshold concentration (Spearman $r = 0.5593$, $p = 0.0634$) but no relationship exists

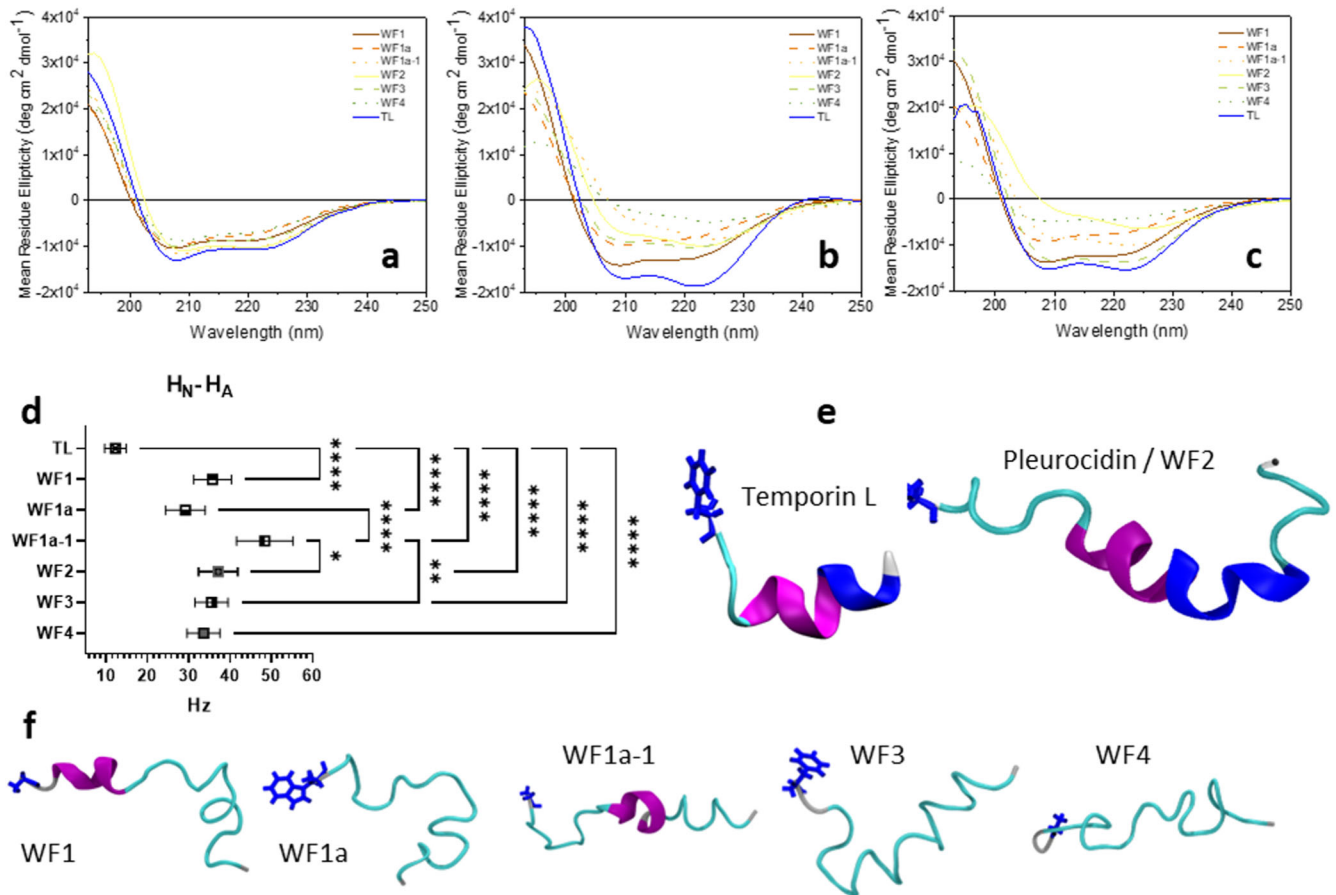


Fig. 3 WF peptides do not adopt ideal α -helix conformations in models of bacterial plasma membranes. Far-UV circular dichroism spectra of 50 μ M Winter Flounder peptides or temporin L in 5 mM Tris buffer at pH 7.5 with 5 mM SDS micelles (a) or 15 μ M in models of Gram-positive (3 mM POPG—b) or Gram-negative (3 mM POPE:POPG (75:25)—c) bacterial plasma membranes at 37 °C. Spectra are representative of three independently repeated experiments. A comparison of H_N to H_A NOESY cross peak linewidths (mean and SD) for WF AMPs and temporin L (TL) in SDS_{d25} reveals much greater linewidths for the WF peptides, indicative of intermediate exchange (d). Newly solved structures of the WF AMPs are likely hybrids of at least two conformations adopted in SDS (f) and lower proportions of α -helix conformation are identified relative to previously solved structures of WF2 (2LS9) and, particularly, temporin L (6GS5) (e). Segments are coloured purple for α -helix, blue for 3-₁₀ helix and cyan and white respectively for turns and coils. Note however that Define Secondary Structure of Proteins (DSSP) is incapable of identifying P_{II} conformation. One-way ANOVA with Bonferroni's multiple comparisons test: * $p < 0.05$; ** $p < 0.01$; **** $p < 0.0001$.

between the threshold concentration and the average MICs for Gram-positive or Gram-negative isolates (Fig. 6b). Therefore, while the ion conductance measurements appear sensitive to variations in the abilities of the WF to penetrate and disorder lipids in model bilayers, such differences do not explain the varying antibacterial potencies.

A better understanding is obtained when the nature of the activity observed at the threshold concentrations is considered as there is substantial variation in the type of activity, the frequency of conductance events, the magnitude of conductance and also the speed with which activity begins after challenge according to the WF AMP applied (Fig. 6c–h and Supplementary Fig. 14). When challenging DPhPG bilayers, modelling Gram-positive bacteria plasma membranes, WF1, WF1a and WF4 have little impact (Fig. 6f) while the onset of activity for WF3 is very slow (Supplementary Fig. 14A). The DPhPE/DPhPG bilayers are generally more resistant to WF AMP induced conductance with only WF1a-1, WF4 and WF2 inducing many high amplitude conductance events (Fig. 6g), while the activity induced by WF2 is slow to begin (Fig. 6d and Supplementary Fig. 14B). Since only these peptides have potent activity against Gram-negative bacteria, these observations are consistent with the relative antibacterial potencies of the WF AMPs described above.

We then focused on whether synergism between WF1a and WF2 can be at all explained by changes in ion conductance. WF1a has very little impact at its threshold concentration (Fig. 6c, g) but when combined with WF2, even at lower concentrations, ion conductance is then substantial (Fig. 6e), with many more high amplitude conductance events (Fig. 6g) and the activity consistently begins much more rapidly (Fig. 6h), the latter being an emergent property since, although this is not significantly faster than when WF1a is used alone ($p = 0.0658$), WF1a alone does not induce conductance that would be associated with bactericidal activity.

DISCUSSION

In the present study, we show that synergy between AMPs found in the Winter Flounder increases potency, enhances cooperativity in the pharmacodynamics of the bactericidal activity and improves therapeutic outcomes in a model of *A. baumannii* wound infection. We further present a first examination of some of the mechanisms that may underpin the synergy and provide insight into how less active WF AMPs—WF1a or WF3—can modulate the membrane interaction of more active WF AMPs—WF2/pleurocidin or WF4. While successful therapy of infected burn wounds in an invertebrate infection model raises the prospect of translating this

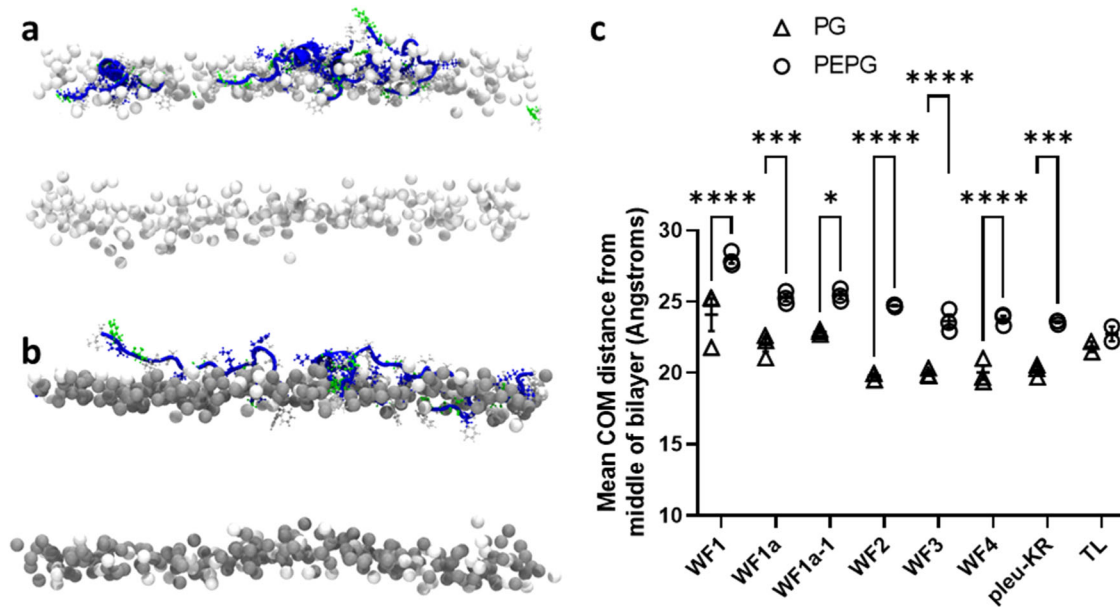


Fig. 4 MD simulation—WF peptides penetrate POPG bilayers more readily than POPE/POPG bilayers. Sideview snapshots for WF2/pleurocidin after 200 ns in POPG (a) or POPE/POPG (b) bilayers—for clarity only the phosphorus atoms are shown for the lipids. Centre of Mass (COM) is shown as averages of the four peptides in each simulation over the last 100 ns in each of three (WF and pleu-KR) or two (temporin L) replicate 200 ns simulations (c). Mean and SE shown for replicates. Two-way ANOVA with Šídák's multiple comparisons test: * $p < 0.05$; ** $p < 0.01$; *** $p < 0.001$; **** $p < 0.0001$.

to mammalian models and, ultimately the clinic, there remain more fundamental questions. These include whether WF AMPs can participate in emergent synergy in higher order combinations and the extent to which variations in environment, bacterial species and strain might affect cooperativity in bactericidal activity and whether this does indeed affect risk and/or frequency of resistance.

The identification of numerous two-way synergistic combinations of WF AMPs can be achieved using both the elegant and efficient approach of Tekin *et al.* and a simple broth microdilution of WF AMPs paired according to their individual MICs. In contrast with Tekin *et al.*, we are unable to identify emergent higher order synergistic combinations, but this may reflect the rapidly bactericidal and high cooperativity of AMP activity. The approach is dependent on identifying antibiotic doses that lead to small but measurable reductions in growth such that even with higher-order combinations, emergent synergism can be identified provided lower-order combinations do not generate complete inhibition¹⁹. However, because of the high cooperativity of AMPs, it is possible for a drastic change in bactericidal activity to be achieved with only a small change in AMP concentration. Indeed, it is possible for zero inhibition to be observed with individual WF AMPs and for near total inhibition to be found with only two-way combinations and we show here that cooperativity is enhanced even with two-way combinations. As such we will likely need a different approach to identify higher order synergy between AMPs with the ideal method both being high throughput and capable of providing dose-dependent and time-resolved data to account for any emergent changes in bactericidal killing rate.

In the interim however MD simulations suggest three-way combinations that should be investigated further. Notably, the MD simulations reveal the peptide-lipid hydrogen bonding patterns of both WF2/pleurocidin and WF4 are similarly affected by the presence of WF3 and hence the question arises as to whether WF3 can affect both peptides simultaneously and what the outcome will be of having these two effects in parallel. In contrast, the effects of WF1a and WF3 on the peptide-lipid hydrogen-bonding pattern of WF2/pleurocidin differ substantially. As such the

question arises whether these effects might compete, or whether some other behaviour emerges. Notably both WF2 and WF3 are expressed in the gills of the Winter Flounder (along with WF1)³³, and WF2, WF3 and WF1a are expressed in the intestine and this raises the question as to how environment and/or differences in bacterial threat shape the function of different synergistic combinations. Expression of WF4 was not found in the adult skin or intestine but other tissues and life stages were not sampled and there was no pathogen insult that might trigger expression³³. The physiological role of WF4 and the combinations in which it might participate therefore remain elusive for now. Nevertheless, it appears likely that co-expression of WF2 with WF1a and/or WF3 in situ can afford gains for the Winter Flounder innate immune system in terms of antibacterial potency which may translate to greater selectivity and reduced collateral damage at the site of infection. Further, while it is yet to be tested, according to the theory advanced by Rolff and others^{1,2,34}, the increase in cooperativity of the bactericidal action obtained by combining different WF AMPs may limit the development of resistance to the Winter Flounder's innate immune response.

In the present study, we are able to establish that poorly active WF AMPs such as WF3 or WF1a are able to modulate the membrane interaction of more active WF AMPs such as WF4 or WF2/pleurocidin. We further show that only those WF AMPs that induce substantial membrane activity at their threshold concentrations have potent antibacterial activity and that this activity is potentiated and accelerated at lower doses of WF2/pleurocidin by WF1a. This effect likely explains the synergistic gain in potency observed in this combination and yet the Gram-negative MICs for both WF2 and WF1a-1 are both well below the threshold concentration in patch-clamp. This would indicate that there is more to the bactericidal mechanism than membrane disruption for both peptides and also that for some bacterial species membrane disruption is a less efficient bactericidal strategy. Therefore, since the ability of WF2/pleurocidin to penetrate bacteria and disrupt intracellular targets is well established for WF2/pleurocidin^{11–13}, and no similar study exists for WF1a-1, there

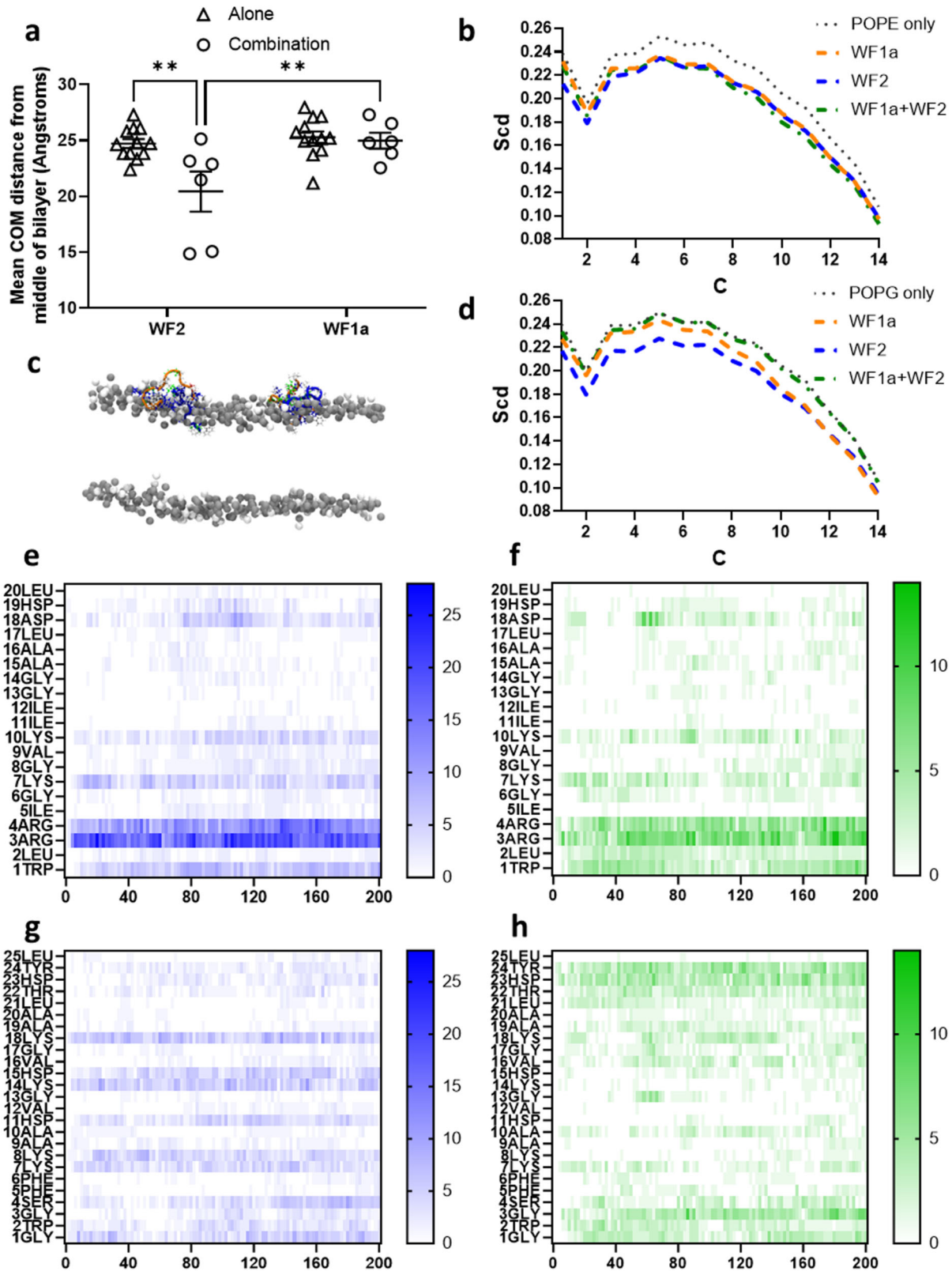


Fig. 5 MD simulation—altered penetration and H-bonding distribution in synergistic combinations of WF2 and WF1a inserting into POPE/POPG bilayers. Centre of mass analysis where each point is one peptide in one of three replicate simulations, the bar is the mean and error is SE (a). Sideview snapshot for WF1a/pleurocidin after 200 ns (c). Lipid acyl chain order parameters for lipids within 4 Å of a peptide shown as averages of the three replicates for POPE (b) or POPG (d) in mixed POPE/POPG bilayers. Hydrogen bonding distribution for WF1a (e, f) or WF2 (g, h) run unmixed (e, g) or as combinations (f, h). Each panel is a sum of four peptides when the peptides are unmixed or two peptides each for the combinations and is representative of $n = 3$ replicates. Two-way ANOVA with Šidák's multiple comparisons test: ** $p < 0.01$.

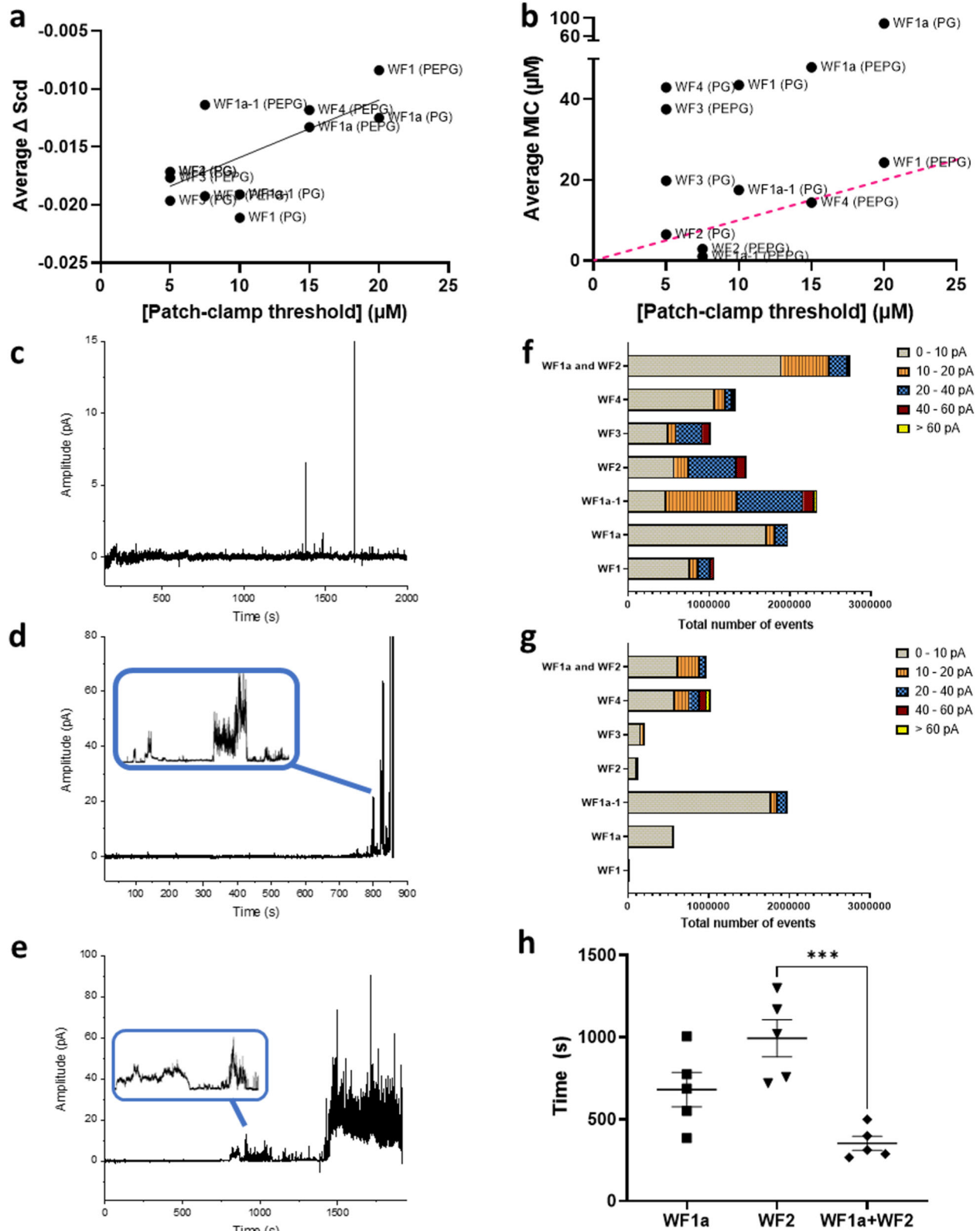


Fig. 6 Ion conductance is sensitive to lipid acyl chain disordering induced by WF AMPs and explains synergistic gain in potency. Disorder of lipid acyl chains induced by WF AMPs in MD simulations is related to the lowest concentration at which ion conductance is detected by patch-clamp (**a** Pearson $r = 0.7007$, $p = 0.0111$). At these concentrations, only some WF AMPs trigger substantial membrane activity (**f** DPhPG; **g** DPhPE/DPhPG) and average MICs for Gram-positive or Gram-negative bacteria are unrelated to these threshold concentrations (**b** Pearson $r = 0.4802$; $p = 0.1141$; red dash = line of identity). At its threshold concentration (7.5 μM) WF2, **d**, **g** induces substantial ion conductance in DPhPE/DPhPG bilayers but this is slow (**d**, **h**) and precedes bilayer disruption. WF1a (15 μM) is largely inert (**c**, **g**). Combining WF2 (3.75 μM) and WF1a (5 μM) ensures substantial ion conductance is induced more rapidly and with less peptide (**e**, **g**, **h**). Time taken to onset of conductance (**h**) is the average and SE of five independent replicates. One-way ANOVA with Bonferroni's multiple comparisons test: *** $p < 0.001$.

is a need to probe non-membrane related contributions to potency and synergy in more depth to fully understand the effect.

While WF AMP effects beyond the bacterial plasma membrane may also influence the cooperativity of bactericidal action—indeed the high cooperativity of gentamicin observed here is consistent with high cooperativity of its binding to two of three classes of binding site on the 70 S ribosome³⁵—the ability of MD simulations to identify modulation of WF4 and WF2/pleurocidin binding and insertion in models of the plasma membrane, by WF1a and/or WF3 suggests that this technique may reveal at least part of how the bactericidal pharmacodynamics are altered in two-way combinations. Enhanced cooperativity in bactericidal activity in two-way synergistic combinations requires a relative inhibition of activity at low AMP concentrations and enhancement of activity at higher concentrations. Features that could support each of these effects are observed at the single concentration tested here, notably the perturbation of the peptide-lipid hydrogen bonding pattern observed for WF2/pleurocidin and WF4 in unmixed condition but also the increased penetration of WF2 (with WF1a) and WF4 (with WF3). Dose dependent changes in this behaviour may therefore provide a mechanistic understanding of the importance of these effects and may be combined with dose dependent, time resolved studies of plasma membrane depolarisation and intracellular target disruption to gain a comprehensive understanding of cooperativity and speed of bactericidal action.

We also show here that the ability to adopt both α -helix and polyproline-II conformations in membrane environments is a distinctive feature of WF AMPs. However, its importance is not yet understood as, although the WF AMPs may penetrate phosphatidylglycerol rich bilayers more readily than other AMPs that adopt only α -helix conformations, we have yet to establish any particular benefit of the P_{II} conformation or the ability to swap between the two conformations or any change in this behaviour in WF AMP combinations (beyond a modest reduction in flexibility for WF1a).

In comparing the cooperativity of WF AMP bactericidal activity between bacterial species and between different strains of *A. baumannii*, we can show that the antibacterial pharmacodynamics of AMPs will be strongly influenced by the nature of the bacterial target. The pharmacodynamics of bactericidal action can both improve or deteriorate following antibiotic adaptation³⁶, and origin of the lower cooperativity observed here for WF AMPs against the more antibiotic resistant AYE strain, relative to *A. baumannii* ACTCC 19778, warrants further investigation.

In summary, we find that synergy can enhance the potency and bactericidal pharmacodynamics of AMPs from the same organism and expressed in the same tissue and this enhances therapy. The PD profile may however vary according to species and/or strain and there is a need to identify contributions both from bacteria and their environment and the AMPs themselves to understand how PD is manipulated. With such an understanding an investigation of whether and how a varying PD profile is indeed linked to resistance risk can follow and the benefits fully appreciated.

METHODS

Peptides and lipids

All peptides were purchased from Cambridge Research Biochemicals (Cleveland, UK) as desalted grade (crude). The crude peptides were further purified using water/acetonitrile gradients using a Waters SymmetryPrep C8, 7 μ m, 19 \times 300 mm column. All peptides were amidated at the C-terminus. The lipids 1-palmitoyl-2-oleoyl-*sn*-glycero-3-phospho-(1'-*rac*-glycerol) (POPG), 1-palmitoyl-2-oleoyl-*sn*-glycero-3-phosphoethanolamine (POPE), 1,2-diphytanoyl-*sn*-glycero-3-phospho-(1'-*rac*-glycerol) (DPhPG) and 1,2-diphytanoyl-*sn*-glycero-3-phosphoethanolamine (DPhPE) were purchased from Avanti Polar

Lipids, Inc. (Alabaster, AL) and used without any purification. All other reagents were used as analytical grade or better. Bacterial isolates are from a collection maintained by UKHSA¹⁴.

Antibacterial activity assay

The antibacterial activity of the peptides was assessed through a modified two-fold broth microdilution assay with modal MICs generated from at least three biological replicate experiments³⁷. The method broadly followed EUCAST methodology, with non-cation adjusted Mueller Hinton replacing cation-adjusted Mueller Hinton. Peptides and antibiotics were diluted in a two-fold dilution in media down a 96 well plate. Bacteria were then added, back-diluted from an overnight culture, at a starting concentration of 5×10^5 CFU/ml. Plates were incubated, static at 37 °C, for 20 h and the OD₆₀₀ was determined using a Clariostar plate reader (BMG Labtech). The MIC was defined as the lowest concentration where growth was <0.1 above the background absorbance.

High order synergy screen

The method of Tekin et al. was followed under the same conditions are the MICs¹⁹. Briefly, an antibacterial activity assay was performed in triplicate as above, and the endpoint growth was used to calculate the peptide concentration which inhibited 10% of growth. Peptides at these concentrations were added to wells of a 96-well plate both alone and in combinations of 2, 3, 4, 5 or all 6 peptides to an accumulative total of 100 μ l. 100 μ l of bacteria at a starting concentration of 5×10^5 CFU/ml were then added and the plate was incubated static at 37 °C for 20 h. The OD₆₀₀ was determined using a Clariostar plate reader (BMG Labtech). The percentage growth inhibition was calculated for each combination compared to an untreated control. Bliss net independence synergy was calculated according to Tekin et al. by subtracting the additive inhibition of the individual peptides from the total inhibition of the combination.

Synergy screen against three isolates

Pair-wise combinations of peptides were tested following an adjusted MIC method as follows. Combinations of 2 peptides, with each compound at its MIC concentration, were added to the first row of a 96-well plate and diluted down the plate in a two-fold serial dilution. Bacteria were added as in a standard MIC assay, the plate was incubated under the same conditions and the MIC of the combination was defined in the same way. The fractional inhibitory concentration was calculated from the combination MIC for two independent repeats, and presented as the average \pm standard error of the mean. FIC is calculated as (MIC of compound A in combination with B/MIC of compound A alone) + (MIC of compound B in combination with A/MIC of compound B alone). Where the MIC was >128 μ g/ml, an assumed MIC of 256 μ g/ml was used to calculate the FIC and a top concentration of 128 μ g/ml was added in the combination. FIC values ≤ 0.5 were considered strongly synergistic and, consistent with a recent re-evaluation of FIC which stresses the importance of also measuring the MIC in the same microarray plate, values of $0.5 < \text{FIC} < 1$ were weakly synergistic¹⁸.

Chequerboard assays

Synergy was measured using standard microdilution Chequerboard assays under the same conditions as the MICs with RPMI140 + 5% FBS used alongside MHB¹⁸. Twofold dilution series of each peptide or antibiotic were prepared in separate 96 well plates and then combined into one before addition of bacteria. The growth/no growth interface was determined using the same definition as the MIC. The fractional inhibitory concentration was calculated from the most synergistic well on the plate for three independent repeats, and presented as above. MICs were

determined on the same plates as the FICs to increase reproducibility.

In vitro pharmacodynamic assay

In vitro pharmacodynamic assays were performed with epidemic methicillin resistant *S. aureus* 15 (EMRSA-15 NCTC 13616) cultured in RPMI140 + 5% FBS or in Mueller-Hinton broth, and *A. baumannii* ATCC 17978 or AYE cultured in Mueller Hinton Broth (MHB). Cation adjusted MHB (CA-MHB) was used when testing daptomycin due to its requirement for Ca^{2+} ions for activity. Bacteria were cultured overnight in 10 ml of MHB or RPMI + 5% FBS at 37 °C and diluted just prior to plate inoculation to an OD_{600} of 0.002. Stock solutions of WF1a, WF2, WF3, WF4, D-WF1a, D-WF2, tobramycin, gentamicin, daptomycin, imipenem, meropenem, or ciprofloxacin were prepared in sterile Milli-Q water at a concentration of 200× MIC. Daptomycin was prepared in methanol at a concentration of 2000× MIC and diluted with media to 200× MIC in the first well. A dilution series was made in the top row of a polypropylene 96-well plate from 200× or 100× MIC (see Supplementary Table 5 for top concentrations for each condition) to 0.2× MIC in a volume of 100 µl, to which 100 µl of the bacterial suspension was added to have a total of 1×10^6 log-phase colony forming units (CFU) in 200 µl. The first $t=0$ sample was taken <30 s after addition of bacteria to the plate with further samples taken at appropriate intervals thereafter. Peptide-challenged bacteria were sampled every 20 min for 120 min due to rapid killing while tobramycin, gentamicin, daptomycin, imipenem, meropenem and ciprofloxacin challenged bacteria were sampled every hour for 6 h. A volume of 15 µl was removed from each well and, following the drop plate method for enumerating bacteria³⁸, diluted 1:1000 in phosphate buffered saline and plated onto MH agar or CA-MH agar plates. The plates were incubated at 37 °C overnight for CFU counting. CFU data were \log_{10} transformed, and the bacterial net growth rate was determined from the increase or decrease in CFU during the time of exposure to the peptides or antibiotics as the coefficient of a linear regression of \log_{10} CFU as a function of time. The intercept of the regression was fixed by forcing the regression lines through the first CFU measurement (0 min) at a given antimicrobial concentration. The pharmacodynamic function according to Regoes et al. describes the relationship between bacterial net growth rate ψ and the concentration of an antimicrobial (a)³⁹:

$$\psi(a) = \psi_{\max} - \frac{(\psi_{\max} - \psi_{\min}) \left(\frac{a}{z\text{MIC}}\right)^{\kappa}}{\left(\frac{a}{z\text{MIC}}\right)^{\kappa} - \frac{\psi_{\min}}{\psi_{\max}}}$$

Fitting this function to the net bacterial growth rates in OriginPro 2020 (OriginLab Corporation, Northampton, MA) generates parameters ψ_{\min} and ψ_{\max} , respectively, the minimum and maximum growth rate, $z\text{MIC}$, the pharmacodynamic minimum inhibitory concentration, and κ , a measure of the cooperativity. Average parameters obtained from fits of three or more independently repeated experiments were compared by one-way ANOVA with a Tukey post hoc test. Since the CFU data is \log_{10} transformed, the net growth rates, are thereafter reported to three significant figures.

Galleria mellonella burn wound infection model

The antimicrobial activities of WF AMPs and the clinically relevant antibiotics gentamicin, ciprofloxacin, imipenem and meropenem against a burn wound infection with *A. baumannii* ATCC 17978 were tested in *Galleria mellonella* larvae. Prior to use, *G. mellonella* were surface decontaminated by immersion in 50% ethanol for 20 s and allowed to dry. All assays were performed on three separate occasions using a group size of 10 larvae; the larvae were kept in separate petri dishes and in the dark in a static incubator at 37 °C for the duration of the experiment. Fresh agar plates of *A.*

baumannii ATCC 17978 were prepared immediately prior to the experiment. Larvae were burnt using the flat head of a nail which was heated in a blue Bunsen burner flame until red hot, cooled for 15 s and superficially applied for 2 s to generate a 2 mm² burn. Larvae were infected with a single colony of *A. baumannii* ATCC 17978 applied directly to the burn site. Treatment was applied topically 1 h after infection in a volume of 5 µl or sterile phosphate buffered saline as a control. Survival was monitored over 96 h.

NMR structure determination

The NMR samples consisted of a 0.5 mM peptide solution also containing 50 mM deuterated sodium dodecyl sulphate (SDS- d_{25}) with 5 mM Tris(hydroxymethyl- d_3)-amino- d_2 -methane buffer at pH 7. 10% D_2O containing trimethylsilyl propanoic acid (TSP) was added for the lock signal and as internal chemical shift reference. The temperature was kept constant at 298 K during the NMR experiments. NMR spectra were acquired on a Bruker Avance 600 MHz (WF1a uniquely at 700 MHz) spectrometer (Bruker, Coventry, UK) equipped with a cryoprobe. Standard Bruker TOCSY and NOESY pulse sequences were used, with water suppression using a WATERGATE 3-9-19 sequence with gradients (mlevgpph19 and noesygpph19). The ^1H 90 degree pulse was calibrated at 37.04 kHz. The TOCSY mixing time was 80 ms, and the mixing time for the NOESY spectra was set to 200 ms. The relaxation delay was 1 s. 2048 data points were recorded in the direct dimension, and 512 data points in the indirect dimension. The spectra were processed using Bruker TOPSPIN. The free induction decay was multiplied by a shifted-sine² window function. After Fourier transformation, the spectra were phase corrected, a baseline correction was applied, and spectra were calibrated to the TSP signal at 0 ppm.

Dynamo⁴⁰ software was used for assignments and structure calculation. Inter-proton NOEs interactions were used as distance restraints in the structure calculation with the annealing protocol in Dynamo. Unambiguous NOEs only were used in this case, after being classified as strong, medium and weak on the base of their relative intensity in the NOESY spectra. Using this classification, upper limits of 0.27, 0.33 and 0.50 nm were applied, respectively, as restraint on the corresponding inter-proton distance. One thousand structures were calculated and the 100 conformers with the lowest potential energy were selected, aligned, and the root mean square deviation (RMSD) of the backbone heavy atoms calculated with respect to their average structure. Solvent molecules were not included in the calculations. Structural coordinates were deposited in the Protein Data Bank (www.rcsb.org)—see “Data availability” statement.

Molecular dynamics simulations

Simulations were carried out on either the KCL *Rosalind* High Performance Computing (HPC) facility, or Dell Precision quad core T3400 or T3500 workstations equipped with a 1 kW Power supply (PSU) and two NVIDIA PNY GeForce GTX570 or GTX580 graphics cards and occasionally the ARCHER Cray XC30 supercomputer using Gromacs 2018 or 2020⁴¹. The CHARMM36 all-atom force field was used in all simulations^{42–44}. All membranes in this project contained a total of 512 lipids, composed either of POPE/POPG (75:25 mol:mol) or POPG. Four peptides were inserted at least 30 Angstrom above the lipid bilayer in a random position and orientation, at least 20 Angstrom apart. The starting structures were taken from the NMR calculation in SDS micelles. As previously, histidine residues were protonated¹⁴, but aspartate or glutamate residues were left in their anionic forms. The system was solvated with TIP3P water and Na^+ ions added to neutralise. Energy minimisation was carried out at 310 K with the Nose–Hoover thermostat using the steepest descent algorithm until the maximum force was less than 1000.0 kJ/ml/nm (<4000 steps). Equilibration was carried out using the NVT

ensemble for 100 ps and then the NPT ensemble for 1000 ps with position restraints on the peptides. Hydrogen-containing bond angles were constrained with the LINCS algorithm. Final simulations were run in the NPT ensemble using 2 fs intervals, with trajectories recorded every 2 ps. All simulations were run in triplicate for a total of 200 ns with peptides inserted at different positions and orientations, giving a total of approximately 10.8 μ s simulation. Torsion angles are circular quantities, and the circular mean of psi or phi angles may be calculated as follows:

$$\bar{\psi} = \text{atan2} \left(\frac{1}{n} \sum_{j=1}^n \sin \psi_j, \frac{1}{n} \sum_{j=1}^n \cos \psi_j \right)$$

Similarly, the associated circular variance for psi or phi angles is calculated as follows:

$$\text{Var}(\psi) = 1 - R_{\text{av}}$$

with R being given by:

$$R^2 = \left(\sum_{i=1}^n \cos \psi_i \right)^2 + \left(\sum_{i=1}^n \sin \psi_i \right)^2$$

Liposome preparation and circular dichroism spectroscopy

Far-UV CD spectra of the peptides bound to small unilamellar vesicles (SUV) were obtained using a Chirascan Plus spectrometer (Applied Photophysics, Leatherhead, UK) with samples maintained at 310 K. To prepare SUV, lipid powders were solubilized in chloroform and dried under rotor-evaporation. To completely remove the organic solvent, the lipid films were left overnight under vacuum and hydrate in 5 mM Tris buffer (pH 7.0). The lipid suspension was subjected to 5 rapid freeze-thaw cycles for further sample homogenisation. POPE/POPG (75:25, mol:mol) and POPG SUVs were obtained by sonicating the lipid suspension on Soniprep 150 (Measuring and Scientific Equipment, London, UK) for 3 \times 5 min with amplitude of 6 microns in the presence of ice to avoid lipid degradation. The SUVs were stored at 4 $^{\circ}$ C and used within 5 days of preparation. Far-UV CD spectra were recorded from 260 to 190 nm. SUV suspension was added to a 0.5 mm cuvette at a final concentration of 3.0 mM and then a few μ l of a concentrated peptide solution were added and thoroughly mixed to give a final peptide concentration of 15 μ M. The same experimental conditions were used to investigate peptide secondary structure in SDS micelles, while the SDS micelles concentration was 5 mM with 50 μ M peptide. In processing, a spectrum of the peptide free lipid suspension or SDS solution was subtracted and Savitsky–Golay smoothing with a convolution width of 5 points applied.

Electrophysiology experiments (patch-clamp)

As in our earlier work¹⁸, lipids with diphtanoyl chains are used here to form giant unilamellar vesicles (GUV). GUVs composed of DPhPE/DPhPG (60:40, mol:mol) and DPhPG were prepared in the presence of 1 M sorbitol by the electroformation method in an indium-tin oxide (ITO) coated glass chamber connected to the Nanion Vesicle Prep Pro setup (Nanion Technologies GmbH, Munich, Germany) using a peak-to-peak AC voltage of 3 V, at a frequency of 5 Hz, for 120 and 140 min, respectively, at 37 $^{\circ}$ C. Bilayers were formed by adding the GUV solution to a buffer containing 250 mM KCl, 50 mM MgCl₂ and 10 mM Hepes (pH 7.00) onto an aperture in a borosilicate chip (Port-a-Patch[®]; Nanion Technologies) and applying 70–90 mbar negative pressure resulting in a solvent-free membrane with a resistance in the G Ω range. After formation, a small amount of peptide stock solution (in water) was added to 50 μ l of buffer solution to obtain its active concentration. All the experiments were carried on with a positive holding potential of 50 mV. The active concentration, the concentration at which the peptide first showed membrane activity, for each peptide was obtained through a titration

performed in the same conditions. For all the experiments a minimum of 6 concordant repeats was done. Current traces were recorded at a sampling rate of 50 kHz using an EPC-10 amplifier from HEKA Elektronik (Lambrecht, Germany). The system was computer controlled by the PatchControl™ software (Nanion) and GePulse (Michael Pusch, Genoa, Italy). The data were filtered using the built-in Bessel filter of the EPC-10 at a cut-off frequency of 10 kHz. The experiments were performed at room temperature. Data analysis was performed with the pClamp 10 software package (Axon Instruments).

Reporting summary

Further information on research design is available in the Nature Research Reporting Summary linked to this article.

DATA AVAILABILITY

Supplementary Information includes more extensive analysis of the MD simulation data, circular dichroism experiments and further analysis of the patch-clamp data. Structural coordinates were deposited in the Protein Data Bank (www.rcsb.org) and Biological Magnetic Resonance Bank (BMRB; www.bmrwisc.edu) under accession codes of 6S2D, 6RYQ, 6RY9, 6RZ1 and 6RZC (PDB) and 34416, 34411, 34410, 34412, and 34413 (BMRB) for WF1, WF1a, WF1a-1, WF3 and WF4, respectively. In addition to the structural coordinates, the data sets generated during and/or analysed during the current study are available from the corresponding author on reasonable request.

Received: 21 March 2023; Accepted: 23 June 2023;

Published online: 10 August 2023

REFERENCES

1. Yu, G., Baeder, D. Y., Regoes, R. R. & Rolff, J. Combination effects of antimicrobial peptides. *Antimicrob. Agents Chemother.* **60**, 1717–1724 (2016).
2. Yu, G., Baeder, D. Y., Regoes, R. R. & Rolff, J. Predicting drug resistance evolution: insights from antimicrobial peptides and antibiotics. *Proc. Biol. Sci.* **285**, 20172687 (2018).
3. Kubicek-Sutherland, J. Z. et al. Antimicrobial peptide exposure selects for *Staphylococcus aureus* resistance to human defence peptides. *J. Antimicrob. Chemother.* **72**, 115–117 (2017).
4. Jangir, P. K., Ogunlana, L. & MacLean, R. C. Evolutionary constraints on the acquisition of antimicrobial peptide resistance in bacterial pathogens. *Trends Microbiol.* **29**, 1058–1061 (2021).
5. Spohn, R. et al. Integrated evolutionary analysis reveals antimicrobial peptides with limited resistance. *Nat. Commun.* **10**, 4538 (2019).
6. Thomas, J. K. et al. Pharmacodynamic evaluation of factors associated with the development of bacterial resistance in acutely ill patients during therapy. *Antimicrob. Agents Chemother.* **42**, 521–527 (1998).
7. Ferguson, P. N. et al. Temporin B forms hetero-oligomers with temporin L, modifies its membrane activity, and increases the cooperativity of its antibacterial pharmacodynamic profile. *Biochemistry* **61**, 1029–1040 (2022).
8. Cole, A. M., Weis, P. & Diamond, G. Isolation and characterization of pleurocidin, an antimicrobial peptide in the skin secretions of Winter Flounder. *J. Biol. Chem.* **272**, 12008–12013 (1997).
9. Saint, N., Cadiou, H., Bessin, Y. & Molle, G. Antibacterial peptide pleurocidin forms ion channels in planar lipid bilayers. *Biochim. Biophys. Acta* **1564**, 359–364 (2002).
10. Yoshida, K. et al. Interaction of pleurocidin and its analogs with phospholipid membrane and their antibacterial activity. *J. Peptide Res.* **57**, 119–126 (2001).
11. Kozłowska, J. et al. Combined systems approaches reveal highly plastic responses to antimicrobial peptide challenge in *Escherichia coli*. *PLoS Pathogens* **10**, e1004104 (2014).
12. Patrzykat, A., Friedrich, C. L., Zhang, L., Mendoza, V. & Hancock, R. E. W. Sublethal concentrations of Pleurocidin-derived antimicrobial peptides inhibit macromolecular synthesis in *Escherichia coli*. *Antimicrob. Agents Chemother.* **46**, 605–614 (2002).
13. Lan, Y. et al. Structural contributions to the intracellular targeting strategy of antimicrobial peptides. *Biochim. Biophys. Acta* **1798**, 1934–1943 (2010).
14. Manzo, G. et al. A Pleurocidin analogue with greater conformational flexibility, enhanced antimicrobial potency and in vivo therapeutic efficacy. *Commun. Biol.* **3**, 697 (2020).
15. Czaplowski, L. et al. Alternatives to antibiotics—a pipeline portfolio review. *Lancet. Infect. Dis.* **16**, 239–251 (2016).
16. Douglas, S. E., Gallant, J. W., Gong, Z. & Hew, C. Cloning and developmental expression of a family of pleurocidin like antimicrobial peptides from winter

- founder, *Pleuronectes americanus* (Walbaum). *Dev. Compar. Immunol.* **25**, 137–147 (2001).
17. Patrzykat, A., Gallant, J. W., Seo, J.-L., Pytyck, J. & Douglas, S. E. Novel antimicrobial peptides derived from flatfish genes. *Antimicrob. Agents Chemother.* **47**, 2464–2470 (2003).
 18. Fratini, F. et al. A novel interpretation of the Fractional Inhibitory Concentration Index: the case *Origanum vulgare* L. and *Leptospermum scoparium* J. R. et G. Forst essential oils against *Staphylococcus aureus* strains. *Microbiol. Res.* **195**, 11–17 (2017).
 19. Tekin, E. et al. Prevalence and patterns of higher-order drug interactions in *Escherichia coli*. *npj Syst. Biol. Appl.* **4**, 31 (2018).
 20. Manzo, G. et al. Temporin L and aurein 2.5 have identical conformations but subtly distinct membrane and antibacterial activities. *Sci. Rep.* **9**, 10934 (2019).
 21. Manzo, G. et al. Minor sequence modifications in temporin B cause drastic changes in antibacterial potency and selectivity by fundamentally altering membrane activity. *Sci. Rep.* **9**, 1385 (2019).
 22. Di Blasio, S. et al. Bolaamphiphile analogues of 12-bis-THA Cl2 are potent antimicrobial therapeutics with distinct mechanisms of action against bacterial, mycobacterial, and fungal pathogens. *mSphere* **8**, e00508–e00522 (2022).
 23. Maslova, E. et al. An invertebrate burn wound model that recapitulates the hallmarks of burn trauma and infection seen in mammalian models. *Front. Microbiol.* **11**, 998 (2020).
 24. Sani, M.-A. & Separovic, F. How membrane-active peptides get into lipid membranes. *Acc. Chem. Res.* **49**, 1130–1138 (2016).
 25. Strandberg, E. et al. Influence of hydrophobic residues on the activity of the antimicrobial peptide Magainin 2 and its synergy with PGLa. *J. Pept. Sci.* **21**, 436–445 (2015).
 26. Zerweck, J. et al. Homo- and heteromeric interaction strengths of the synergistic antimicrobial peptides PGLa and Magainin 2 in membranes. *Eur. Biophys. J.* **45**, 535–547 (2016).
 27. Zerweck, J. et al. Molecular mechanism of synergy between the antimicrobial peptides PGLa and Magainin 2. *Sci. Rep.* **7**, 13153 (2017).
 28. Aisenbrey, C., Amaro, M., Pospíšil, P., Hof, M. & Bechinger, B. Highly synergistic antimicrobial activity of Magainin 2 and PGLa peptides is rooted in the formation of supramolecular complexes with lipids. *Sci. Rep.* **10**, 11652 (2020).
 29. Ma, W. et al. Individual roles of peptides PGLa and Magainin 2 in synergistic membrane poration. *Langmuir* **36**, 7190–7199 (2020).
 30. Amos, S.-B. T. A. et al. Antimicrobial peptide potency is facilitated by greater conformational flexibility when binding to Gram-negative bacterial inner membranes. *Sci. Rep.* **6**, 37639 (2016).
 31. Lopes, J. L. S., Miles, A. J., Whitmore, L. & Wallace, B. A. Distinct circular dichroism spectroscopic signatures of polyproline II and unordered secondary structures: applications in secondary structure analyses. *Protein Sci.* **23**, 1765–1772 (2014).
 32. Mason, A. J., Marquette, A. & Bechinger, B. Zwitterionic phospholipids and sterols modulate antimicrobial peptide-induced membrane destabilization. *Biophys. J.* **93**, 4289–4299 (2007).
 33. Douglas, S. E., Gallant, J. W., Gong, Z. & Hew, C. Cloning and developmental expression of a family of pleurocidin-like antimicrobial peptides from winter flounder, *Pleuronectes americanus* (Walbaum). *Dev. Comp. Immunol.* **25**, 137–147 (2001).
 34. Lazzarola, B. P., Zasloff, M. & Rolff, J. Antimicrobial peptides: application informed by evolution. *Science* **368**, 487 (2020).
 35. Tangy, F., Moukkadem, M., Vindimian, E., Capmau, M. L. & Le Goffic, F. Mechanism of action of gentamicin components. Characteristics of their binding to *Escherichia coli* ribosomes. *Eur. J. Biochem.* **147**, 381–386 (1985).
 36. El Shazeley, B., Yu, G., Johnston, P. R. & Rolff, J. Resistance evolution against antimicrobial peptides in *Staphylococcus aureus* alters pharmacodynamics beyond the MIC. *Front. Microbiol.* **11**, 103 (2020).
 37. Wiegand, I., Hilpert, K. & Hancock, R. E. Agar and broth dilution methods to determine the minimal inhibitory concentration (MIC) of antimicrobial substances. *Nat. Protoc.* **3**, 163–175 (2008).
 38. Herigstad, B., Hamilton, M. & Heersink, J. How to optimize the drop plate method for enumerating bacteria. *J. Microb. Methods.* **44**, 121–129 (2001).
 39. Regoes, R. R. et al. Pharmacodynamic functions: a multiparameter approach to the design of antibiotic treatment regimens. *Antimicrob. Agents Chemother.* **48**, 3670–3676 (2004).
 40. NIDDK, NIH. Dynamo software: the NMR molecular dynamics and analysis system. <http://spin.niddk.nih.gov/NMRPipe/dynamo> (2023).
 41. Abraham, M. J. et al. GROMACS: high performance molecular simulations through multi-level parallelism from laptops to supercomputers. *SoftwareX* **1**, 19–25 (2015).
 42. Best, R. B. et al. Optimization of the additive CHARMM all-atom protein force field targeting improved sampling of the backbone ϕ , ψ and side-chain χ_1 and χ_2 dihedral angles. *J. Chem. Theory Comput.* **8**, 3257–3273 (2012).
 43. Huang, J. & MacKerell, A. D. CHARMM36 all-atom additive protein force field: validation based on comparison to NMR data. *J. Comput. Chem.* **34**, 2135–2145 (2013).
 44. Lee, J. et al. CHARMM-GUI input generator for NAMD, GROMACS, AMBER, OpenMM, and CHARMM/OpenMM simulations using the CHARMM36 additive force field. *J. Chem. Theory Comput.* **12**, 405–413 (2016).
 45. White, S. H. & Wimley, W. C. Hydrophobic interactions of peptides with membrane interfaces. *Biochim. Biophys. Acta* **1376**, 339–352 (1998).

ACKNOWLEDGEMENTS

NMR experiments described in this paper were carried out using the facilities of the Centre for Biomolecular Spectroscopy, King's College London and supported by Dr Andrew Atkinson. The King's instruments were acquired with a Multi-user Equipment Grant from the Wellcome Trust and an Infrastructure Grant from the British Heart Foundation. The authors acknowledge use of the research computing facility at King's College London, *Rosalind* (<https://rosalind.kcl.ac.uk>), which is delivered in partnership with the National Institute for Health Research (NIHR) Biomedical Research Centres at South London & Maudsley and Guy's & St. Thomas' NHS Foundation Trusts, and part-funded by capital equipment grants from the Maudsley Charity (award 980) and Guy's & St. Thomas' Charity (TR130505). The views expressed are those of the author(s) and not necessarily those of the NHS, the NIHR, King's College London, or the Department of Health and Social Care. This work used the ARCHER UK National Supercomputing Service (<http://www.archer.ac.uk>). C.D.L. acknowledges the stimulating research environment provided by the EPSRC Centre for Doctoral Training in Cross-Disciplinary Approaches to Non-Equilibrium Systems (CANES, EP/L015854/1). P.M.F. was supported by a Health Schools Studentship funded by the EPSRC (EP/M50788X/1). A.J.M. received funding from a NC3Rs Skills & Knowledge Transfer grant (NC/T001240/1). J.R. is supported by a BBSRC LIDo iCASE studentship (2547373). C.H. and M. Clifford were supported by funding from PHE Pipeline fund and latterly by PHE Grant in Aid project 109505.

AUTHOR CONTRIBUTIONS

A.J.M. wrote the main manuscript text, prepared all figures and, together with J.M.S. and C.D.L., designed the research. M. Clarke performed structural NMR studies, patch-clamp studies, CD experiments, *Galleria mellonella* experiments and, together with P.M.F., C.D.L. and B.Y., performed and/or analysed atomistic simulation data. Assisted by B.M., M. Clarke also performed in vitro PD experiments. G.M. designed patch-clamp studies. T.T.B. and A.F.D. assisted in analysis and interpretation of CD measurements. C.K.H., M. Clifford, M. Clarke, J.R. and J.M.S. performed and/or designed in vitro antibacterial assays. All authors approved the manuscript.

COMPETING INTERESTS

The authors declare no competing interests.

ADDITIONAL INFORMATION

Supplementary information The online version contains supplementary material available at <https://doi.org/10.1038/s44259-023-00010-7>.

Correspondence and requests for materials should be addressed to Christian D. Lorenz, J. Mark Sutton or A. James Mason.

Reprints and permission information is available at <http://www.nature.com/reprints>

Publisher's note Springer Nature remains neutral with regard to jurisdictional claims in published maps and institutional affiliations.



Open Access This article is licensed under a Creative Commons Attribution 4.0 International License, which permits use, sharing, adaptation, distribution and reproduction in any medium or format, as long as you give appropriate credit to the original author(s) and the source, provide a link to the Creative Commons license, and indicate if changes were made. The images or other third party material in this article are included in the article's Creative Commons license, unless indicated otherwise in a credit line to the material. If material is not included in the article's Creative Commons license and your intended use is not permitted by statutory regulation or exceeds the permitted use, you will need to obtain permission directly from the copyright holder. To view a copy of this license, visit <http://creativecommons.org/licenses/by/4.0/>.